Commun Nonlinear Sci Numer Simulat 91 (2020) 105444

Contents lists available at ScienceDirect

Commun Nonlinear Sci Numer Simulat

journal homepage: www.elsevier.com/locate/cnsns

Research paper

Positivity preserving schemes for the fractional Klein-Kramers equation with boundaries

Luís Pinto[1], Ercília Sousa[1,*]

University of Coimbra, CMUC, Department of Mathematics, 3001-501 Coimbra, Portugal

ARTICLE INFO

Article history:
Received 22 November 2019
Revised 29 May 2020
Accepted 26 June 2020
Available online 7 July 2020

Keywords:
Fractional derivatives
Finite volume schemes
Positivity preserving schemes
Implicit and explicit schemes
Boundary conditions

ABSTRACT

The fractional Klein-Kramers equation describes the process of subdiffusion in the presence of an external force field in phase space and incorporates a fractional operator in time of order α, $0 < \alpha < 1$. We present a family of finite volume schemes for the fractional Klein-Kramers equation, that includes first or second-order schemes in phase space, and implicit or explicit schemes in time with an order of accuracy that can change between α and $2-\alpha$. It is proved, for the open domain, that the schemes satisfy the positivity preserving property. The positivity preserving property for the explicit schemes imposes a strong condition in the relation between time step, space step and phase step, for small values of α, highlighting the advantage of using implicit schemes in these cases. For a bounded domain in space, two types of boundary conditions are considered, absorbing boundary conditions and reflecting boundary conditions. The inclusion of boundary conditions leads to some technical complications that require changes in the schemes near the boundary. The positivity preserving property holds for the new formulation and the overall accuracy is ensured with the use of non-uniform meshes. Numerical tests are presented in the end to show the convergence of the finite volume schemes.

1. Introduction

The deterministic Klein-Kramers equation describes the motion of particles and its solution is a probability density function that depends on the position x and the velocity space v. It is a fundamental equation in the modeling of many physical processes, such as, the particle escape over a barrier and the first passage time. This equation can be seen as a generalization of the classical Fokker-Planck equation to the phase space by taking into account the position and the velocity of the particles whose mass cannot be neglected. These ideas were introduced by Klein [20] and lately developed by Kramers [22]. The Langevin equation can provide the dynamics foundation for these transport processes, where the friction constant, its connection to the diffusion coefficient and the external force enter through this stochastic differential equation [37]. From the Langevin equation, for large friction constants, we can obtain the Fokker-Planck equation and for the low-friction-limit case, we can obtain the Rayleigh equation. For non-zero friction the process is described by the Klein-Kramers equation. A similar interpretation can be done for the fractional Klein-Kramers equation, as can be seen, for instance in [32]. Its stochas-

* Corresponding author.
E-mail addresses: luisp@mat.uc.pt (L. Pinto), ecs@mat.uc.pt (E. Sousa).

[1] This work was partially supported by the Centre for Mathematics of the University of Coimbra – UIDB/00324/2020, funded by the Portuguese Government through FCT/MCTES.

https://doi.org/10.1016/j.cnsns.2020.105444
1007-5704/

tic structure is discussed in [29] where a numerical solution and an approach by the subordinated Langevin equation are also included. Further details on the physical approach of this equation can be found in [12,31,35].

In this work, we propose positivity preserving schemes to solve the fractional Klein-Kramers equation exhibiting anomalous diffusion, subdiffusion, in an external force field $F_{\text{ext}}(x)$. For the function $u(x, v, t)$ the fractional Klein-Kramers equation [32,33,35] is given by

$$\frac{\partial u}{\partial t} = {}_0D_t^{1-\alpha}\left[-\frac{\partial (vu)}{\partial x} + \frac{\partial}{\partial v}\left(\gamma v - \frac{F_{\text{ext}}(x)}{m}\right)u + \frac{\gamma k_B T_p}{m}\frac{\partial^2 u}{\partial v^2}\right], \tag{1}$$

where γ is the friction constant, m is the mass of the particle, T_p is the temperature of the fluid, k_B is the Boltzmann's constant and $F_{\text{ext}}(x)$ is the external force. The operator ${}_0D_t^{1-\alpha}$ with $0 < \alpha < 1$ stands for the Riemann-Liouville fractional derivative. It includes a slowly decaying memory with a power-law kernel and is defined by

$${}_0D_t^{1-\alpha}u(x, v, t) = \frac{1}{\Gamma(\alpha)}\frac{\partial}{\partial t}\int_0^t (t-s)^{\alpha-1}u(x, v, s)ds,$$

where $\Gamma(\cdot)$ is the Gamma function.

The fractional Klein-Kramers equation describes the position and velocity of the Brownian particle successively immobilized in traps [4,12]. The waiting times when the particle stays motionless are drawn from the power-law probability density function. After each trapping event the particle is released with the same position and velocity that it had prior to the immobilization. The heavy-tailed waiting times considerably slow the overall motion and lead to the sublinear in time mean-square displacement of the particle, which is typical for subdiffusion.

In many physical contexts, random processes can be found whose probability density function is a solution of the fractional Klein-Kramers equation [2,29,31,40] and, therefore, it is important to implement numerical methods that guaranty the numerical solution is non-negative, which will be the focus of our work.

For numerical calculations it is convenient to use the Klein-Kramers equation in normalized form. By introducing the following variables and parameters

$$x_n = \sqrt{\frac{m}{k_B}}x, \quad v_n = \sqrt{\frac{m}{k_B}}v, \quad F_{\text{ext}n}(x_n) = \sqrt{\frac{m}{k_B}}F_{\text{ext}}(x), \tag{2}$$

the fractional Klein-Kramers equation transforms to

$$\frac{\partial u_n}{\partial t} = {}_0D_t^{1-\alpha}\left[-\frac{\partial (v_n u_n)}{\partial x_n} + \frac{\partial}{\partial v_n}(\gamma v_n - F_{\text{ext}n}(x_n))u_n + \gamma T_p\frac{\partial^2 u_n}{\partial v_n^2}\right]. \tag{3}$$

Omitting the subscript n for convenience, the equation under study will be

$$\frac{\partial u}{\partial t} = {}_0D_t^{1-\alpha}\left[-\frac{\partial (vu)}{\partial x} - \frac{\partial}{\partial v}(F(x, v)u) + D\frac{\partial^2 u}{\partial v^2}\right], \tag{4}$$

where

$$F(x, v) = F_{\text{ext}}(x) - \gamma v, \quad D = \gamma T_p. \tag{5}$$

The external force $F_{\text{ext}}(x)$ most of the times depends on a potential field, that is, $F_{\text{ext}}(x) = -V'(x)$.

Eq. (4) can also have a different form that comes from applying the fractional operator ${}_0D_t^{\alpha-1}$ on both sides of the equation. If u is bounded at the lower limit in time then

$${}_0D_t^{\alpha-1}\left({}_0D_t^{1-\alpha}u(x, v, t)\right) = u(x, v, t).$$

These fractional derivatives exist, if the function u is in L^1. A more complete discussion on the regularity of the solutions can be found in [19,34,38]. Additionally, we have

$${}_0D_t^{\alpha-1}\left(\frac{\partial u}{\partial t}(x, v, t)\right) = {}_0^C D_t^{\alpha}u(x, v, t),$$

where the operator ${}_0^C D_t^{\alpha}u$ is the Caputo fractional derivative defined by

$${}_0^C D_t^{\alpha}u(x, v, t) := \frac{1}{\Gamma(1-\alpha)}\int_0^t \frac{\partial u}{\partial t}(x, v, s)(t-s)^{-\alpha}ds.$$

Therefore the fractional Klein-Kramers equation has the form

$${}_0^C D_t^{\alpha}u = -\frac{\partial (vu)}{\partial x} - \frac{\partial}{\partial v}(F(x, v)u) + D\frac{\partial^2 u}{\partial v^2}. \tag{6}$$

The difficulties of solving the Klein-Kramers equation numerically come from several factors. This problem behaves like a parabolic equation in the v-direction, and behaves like a hyperbolic equation in the x-direction. Additionally in the x-direction, depending on the sign of v, the solution may satisfy different kinds of boundary conditions on different subdomains. This leads to additional difficulties in actual computation and theoretical analysis.

The main purpose of this work is to derive positivity preserving finite volume methods, for the fractional Klein-Kramers Eq. (6) and in the presence of physical boundaries. We consider not only the case when we have an open domain, that is, natural boundary conditions, but also the case when we have absorbing and reflecting boundaries in the spatial direction (x-direction). These boundaries are frequently associated with the Klein-Kramers equation as can be seen, for instance, in [1,10,11,37].

The approach presented here, with finite volume methods, allows to get second-order schemes more suitable for problems where the non-diffusive flux term is dominant and in this way it covers the most interesting cases. Additionally the implementation takes into account the presence of physical boundaries. As far as we know there are no works that study numerical solutions for the fractional Klein-Kramers equation in the presence of these boundaries. Only finite difference methods for the fractional Klein-Kramers equation have been considered in literature [6] but not with absorbing or reflecting boundaries. Furthermore in the presence of a dominant force field the positivity preserving finite volume schemes avoid non-physical numerical oscillations that can easily appear with other numerical methods.

Finite volume methods for time fractional differential equations have not been extensively studied either. However some works have appeared recently for fractional differential equations that involve the Caputo fractional derivative, such as, [17,28]. These works consider one dimensional problems and they differ significantly from the work we are presenting since a two dimensional problem is considered that is parabolic in one direction, hyperbolic in another direction and with the additional difficulty of assuming physical boundaries.

The structure of the paper is as follows. In the next section, the finite volume schemes are described in an open domain. Then, in Section 3, the properties of the finite volume methods are presented, that is, we prove the positivity preserving property. In Section 4 we discuss the case of having a bounded domain in the spatial direction (x-direction) and how to reformulate the finite volume schemes in order to maintain the positivity of the numerical solution. In Section 5 numerical tests are presented that show the convergence of the numerical methods, how the presence of boundary conditions affect the accuracy of the finite volume schemes and how to recover the accuracy using a non-uniform mesh. We also show numerical solutions of the Klein-Kramers equations for physically relevant force fields and compare the performance of the methods with an existing method in literature. We finish with some conclusions.

2. The numerical method

We start to discuss finite volume methods for a problem with natural boundary conditions, that is, $\lim_{|x|\to\infty} u(x,v,t) = 0, \lim_{|v|\to\infty} u(x,v,t) = 0$.

The finite volume methods will be first-order or second-order in phase space and the approach follows the ideas presented in [5,23,24]. For the time discretization we consider an explicit method, an implicit method and an implicit-explicit (IMEX) method. The discretisation in time will have an order of accuracy that can be between α and $2-\alpha$ according to the regularity of the solution and depending on the type of temporal mesh. These schemes will be positivity preserving, which is a physical property required by Eq. (6) for suitable initial and boundary conditions. The time discretisation is also chosen to ensure that the positivity preserving property holds.

2.1. Finite volume method: spatial discretisation

Consider the spatial domain $\Omega = [x_L, x_R] \times [v_L, v_R]$ and let $(x_i,\ v_j)$, $i = 1,\dots,N_x;\ j = 1,\dots,N_v$ denote a vertex-centered discretization of Ω. For reasons that will become clear later on, we consider a uniform-discretization in the v-direction (phase direction) and a non-uniform discretization in the x-direction (spatial direction). In particular, we define $x_{i+1} = x_i + \Delta x_i$, with $x_1 = x_L$, $x_{N_x} = x_R$ and $v_{j+1} = v_j + \Delta v$, with $v_1 = v_L$, $v_{N_v} = v_R$.

Associated with this discretization we define the cell-centered finite volume grid $(\bar{x}_i, \bar{v}_j)$, $i = 1,\dots,N_x - 1;\ j = 1,\dots,N_v - 1$ with $\bar{x}_i = x_i + \Delta x_i/2$ and $\bar{v}_j = v_j + \Delta v/2$. We define the cells $C_{i,j} = [\bar{x}_{i-1/2,j}, \bar{v}_{i,j-1/2}] \times [\bar{x}_{i+1/2,j}, \bar{v}_{i,j+1/2}]$, $i = 1,\dots,N_x - 1$, $j = 1,\dots,N_v - 1$, where $\bar{x}_{i\pm1/2,j} = \bar{x}_{i,j} \pm \Delta x_i/2$ and $\bar{v}_{i,j\pm1/2} = \bar{v}_{i,j} \pm \Delta v/2$. Note that the cell boundary points $(\bar{x}_{i\pm1/2,j}, \bar{v}_{i,j\pm1/2})$ coincide with the vertex-centered grid points $(x_i,\ v_j)$, as displayed in Fig. 1(a). In the following, unless otherwise specified, the subscripts i, j are used to denote an approximation at the node $(\bar{x}_i, \bar{v}_j)$. Similarly, the subscripts $i \pm 1/2, j$ and $i, j \pm 1/2$ denote an approximation at the nodes $(\bar{x}_{i\pm1/2}, \bar{v}_j)$ and $(\bar{x}_i, \bar{v}_{j\pm1/2})$ respectively.

Let us define the flux functions $f_u^x(x,v,t) = vu$ and $g_u^v(x,v,t) = F(x,v)u$. We start with a standard finite volume approach and integrate (6) over a cell C_{ij}. Multiplying on both sides by $1/\Delta x_i \Delta v$, and integrating, we obtain

$$\int_{C_{i,j}} \frac{{}_0^C D_t^\alpha u(x,v,t)}{\Delta x_i \Delta v}\, dx dv = -\int_{\bar{v}_{j-1/2}}^{\bar{v}_{j+1/2}} \frac{f_u^x(\bar{x}_{i+1/2},v,t) - f_u^x(\bar{x}_{i-1/2},v,t)}{\Delta x_i \Delta v}\, dv - \int_{\bar{x}_{i-1/2}}^{\bar{x}_{i+1/2}} \frac{g_u^v(x,\bar{v}_{j+1/2},t) - g_u^v(x,\bar{v}_{j-1/2},t)}{\Delta x_i \Delta v}\, dx$$
$$+ \frac{D}{\Delta x_i \Delta v} \int_{\bar{x}_{i-1/2}}^{\bar{x}_{i+1/2}} \left(\frac{\partial u(x,\bar{v}_{j+1/2},t)}{\partial v} - \frac{\partial u(x,\bar{v}_{j-1/2},t)}{\partial v} \right) dx. \tag{7}$$

We apply the midpoint integration rule on the first and second integral on the right-hand side of Eq. (7). For the third integral the centered finite difference approximation is used

$$\frac{\partial u(x,\bar{v}_{j+1/2},t)}{\partial v} \approx \frac{u(x,\bar{v}_{j+1},t) - u(x,\bar{v}_j,t)}{\Delta v}.$$

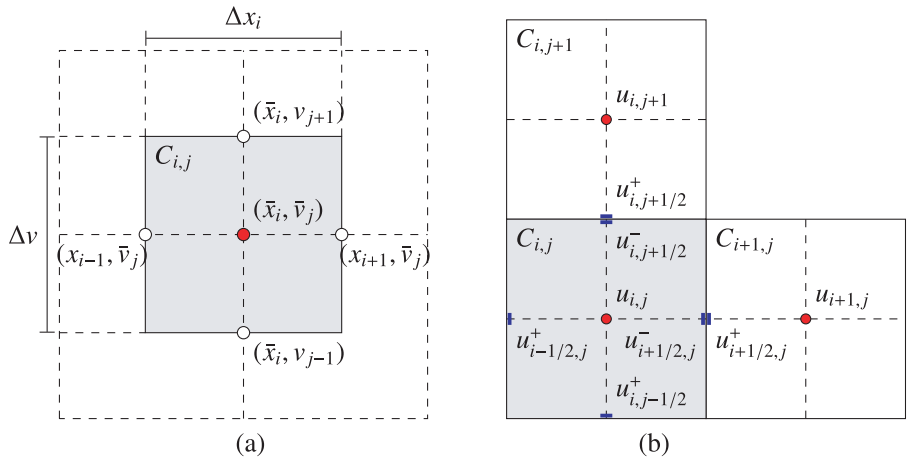

Fig. 1. (a) Volume cell $C_{i,j} = [\bar{x}_{i-1/2}, \bar{x}_{i+1/2}] \times [\bar{v}_{j-1/2}, \bar{v}_{j+1/2}] = [x_i, x_{i+1}] \times [v_j, v_{j+1}]$ centered at $(\bar{x}_i, \bar{v}_j)$. We denote $u_{i,j} = u(\bar{x}_i, \bar{v}_j)$. (b) Reconstructed values $u^{\pm}_{i\pm1/2,j}$, $u^{\pm}_{i,j\pm1/2}$ (in blue) defined according to (11)–(12). They are boundary extrapolated data, computed at the edges of each cell. (For interpretation of the references to colour in this figure legend, the reader is referred to the web version of this article.)

We can also write

$$u(\bar{x}_i, \bar{v}_j, t) \simeq \frac{1}{\Delta x_i \Delta v} \int_{C_{i,j}} u(x, v, t)\, dxdv,$$

and denote the approximated values at the cell centered nodes of u and u_0 as

$$u_{i,j}(t) := u(\bar{x}_i, \bar{v}_j, t), \qquad u^0_{i,j} := u_0(\bar{x}_i, \bar{v}_j).$$

The following numerical method is obtained

$$\begin{aligned} {}_0^C D_t^\alpha u_{i,j}(t) = &- \frac{f^x_u(\bar{x}_{i+1/2}, \bar{v}_j, t) - f^x_u(\bar{x}_{i-1/2}, \bar{v}_j, t)}{\Delta x_i} - \frac{g^v_u(\bar{x}_i, \bar{v}_{j+1/2}, t) - g^v_u(\bar{x}_i, \bar{v}_{j-1/2}, t)}{\Delta v} \\ &+ D \frac{u_{i,j+1}(t) - 2u_{i,j}(t) + u_{i,j-1}(t)}{\Delta v^2}. \end{aligned} \tag{8}$$

To evaluate the flux functions we introduce the quantities $u^{\pm}_{i+1/2,j}(t)$ and $u^{\pm}_{i,j+1/2}(t)$. They are boundary extrapolated data, computed at the edges of each cell with a piecewise linear reconstruction at fixed time t, as illustrated in Fig. 1(b). More details are given after the definition of the fluxes.

The values $f^x_u(\bar{x}_{i+1/2}, \bar{v}_j, t)$ and $g^v_u(\bar{x}_i, \bar{v}_{j+1/2}, t)$ are determined in the following manner,

$$f^x_u(\bar{x}_{i+1/2}, \bar{v}_j, t) \simeq \frac{\bar{v}_j u^+_{i+1/2,j}(t) + \bar{v}_j u^-_{i+1/2,j}(t)}{2} - \frac{a^x_{i+1/2,j}(t)}{2}(u^+_{i+1/2,j}(t) - u^-_{i+1/2,j}(t)), \tag{9}$$

$$g^v_u(\bar{x}_i, \bar{v}_{j+1/2}, t) \simeq \frac{F_{i,j+1/2} u^+_{i,j+1/2}(t) + F_{i,j+1/2} u^-_{i,j+1/2}(t)}{2} - \frac{b^v_{i,j+1/2}(t)}{2}(u^+_{i,j+1/2}(t) - u^-_{i,j+1/2}(t)), \tag{10}$$

where $F_{i,j} := F(\bar{x}_i, \bar{v}_j)$. In (9) and (10), $a^x_{i+1/2,j}(t)$ and $b^v_{i,j+1/2}(t)$ are called local maximal speeds and they are given by

$$a^x_{i+1/2,j}(t) = \left| \frac{\partial f^x_u}{\partial u} \right| = |\bar{v}_j|, \quad b^v_{i,j+1/2}(t) = \left| \frac{\partial g^v_u}{\partial u} \right| = |F_{i,j+1/2}|,$$

with $|\cdot|$ the absolute value.

Let us now define the quantities $u^{\pm}_{i+1/2,j}(t)$ and $u^{\pm}_{i,j+1/2}(t)$. These values represent suitable approximations, first-order or second-order accurate and positivity preserving, for $u(x, v, t)$ at the right (+) and at the left (-) of the points $(\bar{x}_{i+1/2}, \bar{v}_j)$ and $(\bar{x}_i, \bar{v}_{j+1/2})$. The choice of these values can determine if we have a first-order or a second-order finite volume scheme.

We start to describe how we obtain the second-order approximation. We define on each cell $C_{i,j}$ a piecewise linear reconstruction for u, denoted by $\tilde{u}|_{C_{i,j}}$, that reads

$$\tilde{u}|_{C_{i,j}}(x, v, t) = u_{i,j}(t) + (u_x)_{i,j}(t)(x - \bar{x}_i) + (u_v)_{i,j}(t)(v - \bar{v}_j), \quad (x, v) \in C_{i,j}, \tag{11}$$

where $(u_x)_{ij}(t)$ and $(u_v)_{i,j}(t)$ are at least first-order approximations of their respective first-order derivatives, that is,

$$(u_x)_{i,j}(t) \simeq \frac{\partial u}{\partial x}(\bar{x}_i, \bar{v}_j, t), \quad (u_v)_{i,j}(t) \simeq \frac{\partial u}{\partial v}(\bar{x}_i, \bar{v}_j, t).$$

The constructed points $u^{\pm}_{i+1/2,j}$ and $u^{\pm}_{i,j+1/2}$ are then given by

$$u^{-}_{i+1/2,j}(t) = \tilde{u}|_{C_{i,j}}(\bar{x}_i + \Delta x_i/2, \bar{v}_j, t),\ u^{+}_{i+1/2,j}(t) = \tilde{u}|_{C_{i+1,j}}(\bar{x}_{i+1} - \Delta x_{i+1}/2, \bar{v}_j, t),$$
$$u^{-}_{i,j+1/2}(t) = \tilde{u}|_{C_{i,j}}(\bar{x}_i, \bar{v}_j + \Delta v/2, t),\ u^{+}_{i,j+1/2}(t) = \tilde{u}|_{C_{i,j+1}}(\bar{x}_i, \bar{v}_{j+1} - \Delta v/2, t). \tag{12}$$

Further details can be found in [5]. To avoid oscillatory reconstructions and preserve the positivity, the numerical approximations of the derivatives can be computed using a nonlinear limiter. Here the generalized minmod limiter is used [5,23,24], that is, $(u_x)_{i,j}(t)$ and $(u_v)_{i,j}(t)$ are respectively given by

$$\text{minmod}\left(\theta\frac{u_{i,j}(t) - u_{i-1,j}(t)}{\bar{x}_i - \bar{x}_{i-1}}, \frac{u_{i+1,j}(t) - u_{i-1,j}(t)}{\bar{x}_{i+1} - \bar{x}_{i-1}}, \theta\frac{u_{i+1,j}(t) - u_{i,j}(t)}{\bar{x}_{i+1} - \bar{x}_i}\right),$$
$$\text{minmod}\left(\theta\frac{u_{i,j}(t) - u_{i,j-1}(t)}{\bar{v}_j - \bar{v}_{j-1}}, \frac{u_{i,j+1}(t) - u_{i,j-1}(t)}{\bar{v}_{j+1} - \bar{v}_{j-1}}, \theta\frac{u_{i,j+1}(t) - u_{i,j}(t)}{\bar{v}_{j+1} - \bar{v}_j}\right),$$

with the minmod function defined as

$$\text{minmod}(z_1, z_2, \ldots, z_k) = \begin{cases} \min\limits_k z_k, & \text{if } z_k > 0, \text{ for all } k, \\ \max\limits_k z_k, & \text{if } z_k < 0 \text{ for all } k, \\ 0, & \text{otherwise.} \end{cases} \tag{13}$$

The parameter $\theta \in [1, 2]$ is related to the numerical viscosity of the scheme. Larger values originate less dissipative results, however, non-physical numerical oscillations can arise [5,23,24]. The optimal θ value is problem dependent. Here, unless otherwise stated, we consider $\theta = 2$.

This finite volume scheme is theoretically second-order accurate [5,23]. Note however that it reduces to a first-order upwind scheme when the minmod function returns the zero value. In practice this situation may occur near steep gradients or discontinuities.

Remark 1. The numerical fluxes can be rewritten in a different form. If $\bar{v}_j > 0$ then $f^x_u(\bar{x}_{i\pm1/2}, \bar{v}_j, t) \simeq \bar{v}_j u^{-}_{i\pm1/2,j}(t)$ and if $\bar{v}_j \le 0$ then $f^x_u(\bar{x}_{i\pm1/2}, \bar{v}_j, t) \simeq \bar{v}_j u^{+}_{i\pm1/2,j}(t)$. Also, if $F_{i,j+1/2} > 0$ then $g^v_u(\bar{x}_i, \bar{v}_{j+1/2}, t) \simeq F_{i,j+1/2} u^{-}_{i,j+1/2}(t)$ and if $F_{i,j+1/2} \le 0$ then we have $g^v_u(\bar{x}_i, \bar{v}_{j+1/2}, t) \simeq F_{i,j+1/2} u^{+}_{i,j+1/2}(t)$.

Regarding the first-order approximation the values $u^{\pm}_{i+1/2,j}$ and $u^{\pm}_{i-1/2,j}$ are simply given by $u^{+}_{i+1/2,j} = u_{i+1,j},\ u^{-}_{i+1/2,j} = u_{i,j}$, $u^{+}_{i-1/2,j} = u_{i,j},\ u^{+}_{i-1/2,j} = u_{i-1,j}$. The values $u^{\pm}_{i,j\pm1/2}$ are obtained in a similar way.

In the next section we discuss the discretisation in time.

2.2. Time discretisation

In this section we discuss the discretization in time. By introducing the operators

$$L_A u_{i,j}(t) := -\frac{f^x_u(\bar{x}_{i+1/2}, \bar{v}_j, t) - f^x_u(\bar{x}_{i+1/2}, \bar{v}_j, t)}{\Delta x_i} - \frac{g^v_u(\bar{x}_i, \bar{v}_{j+1/2}, t) - g^v_u(\bar{x}_i, \bar{v}_{j-1/2}, t)}{\Delta v}, \tag{14}$$

$$L_D u_{i,j}(t) := D\frac{u_{i,j+1}(t) - 2u_{i,j}(t) + u_{i,j-1}(t)}{\Delta v^2}, \tag{15}$$

we can rewrite the numerical approach (8) as

$${}^{C}_{0}D^{\alpha}_{t} u_{i,j}(t) = L^{\tau}_A u_{i,j}(t) + L_D u_{i,j}(t),\ \tau = 1, 2, \tag{16}$$

where $\tau = 1$ refers to the first-order finite volume approximation of the fluxes and $\tau = 2$ to the second-order approximation. We consider a non-uniform time step discretization $0 = t_0 < t_1 < t_2 < \ldots < t_n = T$ and denote $\Delta t_n = t_n - t_{n-1}$ the time step. The maximum step is denoted by $\Delta t = \max\limits_n \Delta t_n$.

We start to discuss the discretisation of the Caputo fractional derivative. In the last years, several approaches to discretize the Caputo derivative have appeared in the literature [7–9,13,25,30,36], but we will use the $L1$ approximation that recently has received much attention. This approximation is constructed by using a piecewise linear interpolation of the solution on each subinterval. It was proved, in [27], to be of order $O(\Delta t^{2-\alpha})$ for a uniform mesh, if the solution is $C^2([0, T])$. But this assumes that the solution is smooth at the initial time $t = 0$. However, often the solution does not have this type of regularity at $t = 0$. Therefore some recent works have improved such estimates. In [18] it was shown that the L1 formula is accurate of order $O(\Delta t)$ for less smooth functions on a uniform mesh. In [39] error estimates were obtained for the L1 formula on graded time grids, showing how the regularity of the solution and the grading of the mesh affect the order of convergence of the difference scheme. In particular, if the regularity of the solution is reduced we can get order of convergence $O(\Delta t^{\alpha})$. In [26] the L1 formula for approximating the Caputo derivative was revisited and it was shown that the nonuniform L1 scheme achieves an optimal temporal convergence of order $O(\Delta t^{2-\alpha})$ under the graded grid $t_k = T(k/M)^{\gamma opt}$

with M mesh points and an optimal parameter γopt. Also in [21], more discussions about considering non-uniform meshes can be found. In conclusion, we can expect the order of accuracy of the $L1$ approximation to change between Δt^{α} and $\Delta t^{2-\alpha}$ depending on the regularity of the solution and the type of temporal mesh.

The $L1$ approximation can be easily explained. It consists of approximating the derivative inside the integral by a standard first-order approximation and then the integral is computed exactly. If we denote $u_{i,j}^{n} := u_{i,j}(t_n)$, the approximation of the Caputo derivative can be given by

$$D_M^{\alpha} u_{i,j}^{n} = \frac{1}{\Gamma(1-\alpha)} \sum_{k=0}^{n-1} \frac{u_{i,j}^{k+1} - u_{i,j}^{k}}{\Delta t_{k+1}} \int_{t_k}^{t_{k+1}} (t_n - s)^{-\alpha} ds = \frac{1}{\Gamma(2-\alpha)} \sum_{k=0}^{n-1} \frac{u_{i,j}^{k+1} - u_{i,j}^{k}}{\Delta t_{k+1}} [(t_n - t_k)^{1-\alpha} - (t_n - t_{k+1})^{1-\alpha}].$$

This approximation can be re-written as

$$D_M^{\alpha} u_{i,j}^{n} = \frac{d_{n,1}}{\Gamma(2-\alpha)} u_{i,j}^{n} - \frac{d_{n,n}}{\Gamma(2-\alpha)} u_{i,j}^{0} + \frac{1}{\Gamma(2-\alpha)} \sum_{k=1}^{n-1} (d_{n,k+1} - d_{n,k}) u_{i,j}^{n-k}, \tag{17}$$

where

$$d_{n,k} = \frac{(t_n - t_{n-k})^{1-\alpha} - (t_n - t_{n-k+1})^{1-\alpha}}{\Delta t_{n-k+1}}.$$

Simplifying a little more by doing $n - k = p$

$$D_M^{\alpha} u_{i,j}^{n} = \frac{d_{n-1}}{\Gamma(2-\alpha)} u_{i,j}^{n} - \frac{d_0}{\Gamma(2-\alpha)} u_{i,j}^{0} + \frac{1}{\Gamma(2-\alpha)} \sum_{p=1}^{n-1} (d_{p-1} - d_p) u_{i,j}^{p}, \tag{18}$$

where

$$d_{n-1} = \frac{1}{\Delta t_n^{\alpha}}, \quad d_p = \frac{(t_n - t_p)^{1-\alpha} - (t_n - t_{p+1})^{1-\alpha}}{\Delta t_{p+1}}, \ \ p = 0, \ldots, n-2.$$

Since $d_p \geq 0, \ \ p = 0, 1, \ldots, n-1$ and $\ d_{p-1} \leq d_p$, the coefficients of the terms in the last sum of (18) are negative.

A family of numerical methods is presented that are first-order or second-order in phase space and explicit or implicit in time. They consist of an explicit method with the first and second-order finite volume scheme, an IMEX method with the second-order finite volume scheme and an implicit method with the first-order finite volume scheme given respectively by

$$\text{Explicit} \quad D_M^{\alpha} u_{i,j}^{n} = L_A^{\tau} u_{i,j}^{n-1} + L_D u_{i,j}^{n-1}, \quad \tau = 1, 2, \tag{19}$$

$$\text{IMEX} \quad D_M^{\alpha} u_{i,j}^{n} = L_A^{2} u_{i,j}^{n-1} + L_D u_{i,j}^{n}, \tag{20}$$

$$\text{Implicit} \quad D_M^{\alpha} u_{i,j}^{n} = L_A^{1} u_{i,j}^{n} + L_D u_{i,j}^{n}. \tag{21}$$

3. Properties of the finite volume schemes

In the previous section, the schemes were presented and the various aspects of consistency were discussed. The consistency together with stability properties are necessary conditions for the convergence of the finite volume schemes. In this section we prove the positivity preserving property of the numerical solutions which is an important stability property of the method since the appearance of negative values may trigger numerical instabilities [5].

We start to present the results for the explicit method with the second-order finite volume approximation in phase space.

Theorem 1 (Second-order explicit method)**.** *Consider the finite volume scheme (19) for $\tau = 2$. Then the cell values $u_{i,j}(t_n)$ remain nonnegative provided the initial cell values are nonnegative and the following conditions are satisfied, for all $n \geq 1$,*

$$\frac{1}{\Delta t_{n+1/2}} \left(\frac{\Delta t_n^{\alpha} \Delta t_{n-1} \Gamma(2-\alpha)}{2 - 2^{1-\alpha} \left(\Delta t_n / \Delta t_{n+1/2} \right)^{\alpha}} \right) \leq \min \left\{ \frac{\Delta v^2}{2D}(1-w), \frac{\Delta x_m}{v_M} \frac{w}{4}, \frac{\Delta v}{F_M} \frac{w}{4} \right\}, \tag{22}$$

where $0 < w < 1$, $\Delta x_m = \min_i \Delta x_i$, $\Delta t_{n+1/2} = (\Delta t_n + \Delta t_{n-1})/2$, $v_M = \max |v|$ and $F_M = \max |F(x, v)|$.

Proof. In what follows, we consider the reconstructed points $u_{i\pm 1/2, j}^{\pm}(t_{n-1})$ and $u_{i, j\pm 1/2}^{\pm}(t_{n-1})$ and we omit the time step t_{n-1} for the sake of clarity. Let $u_{i,j}^{k} := u_{i,j}(t_k)$. The numerical method (19) as the explicit form

$$\frac{d_{n-1}}{\Gamma(2-\alpha)} u_{i,j}^{n} - \frac{d_0}{\Gamma(2-\alpha)} u_{i,j}^{0} + \frac{1}{\Gamma(2-\alpha)} \sum_{p=1}^{n-1} (d_{p-1} - d_p) u_{i,j}^{p}$$

$$= -\frac{1}{2\Delta x_i}\Big[\bar{v}_j(u^+_{i+1/2,j}+u^-_{i+1/2,j}) - |\bar{v}_j|(u^+_{i+1/2,j}-u^-_{i+1/2,j})$$
$$-\bar{v}_j(u^+_{i-1/2,j}+u^-_{i-1/2,j}) + |\bar{v}_j|(u^+_{i-1/2,j}-u^-_{i-1/2,j})\Big] - \frac{1}{2\Delta v}\Big[F_{i,j+1/2}(u^+_{i,j+1/2}+u^-_{i,j+1/2}) - |F_{i,j+1/2}|(u^+_{i,j+1/2}-u^-_{i,j+1/2})$$
$$-F_{i,j-1/2}(u^+_{i,j-1/2}+u^-_{i,j-1/2}) + |F_{i,j-1/2}|(u^+_{i,j-1/2}-u^-_{i,j-1/2})\Big] + \frac{D}{\Delta v^2}(u^{n-1}_{i,j+1} - 2u^{n-1}_{i,j} + u^{n-1}_{i,j-1}).$$

Rearranging the terms we have the following linear combination

$$\frac{d_{n-1}}{\Gamma(2-\alpha)}u^n_{i,j} = \frac{d_0}{\Gamma(2-\alpha)}u^0_{i,j} - \sum_{p=1}^{n-2}\frac{(d_{p-1}-d_p)}{\Gamma(2-\alpha)}u^p_{i,j} - \frac{(d_{n-2}-d_{n-1})}{\Gamma(2-\alpha)}u^{n-1}_{i,j} + u^+_{i+1/2,j}\frac{-\bar{v}_j+|\bar{v}_j|}{2\Delta x_i} + u^-_{i+1/2,j}\frac{-\bar{v}_j-|\bar{v}_j|}{2\Delta x_i}$$
$$+ u^+_{i-1/2,j}\frac{\bar{v}_j-|\bar{v}_j|}{2\Delta x_i} + u^-_{i-1/2,j}\frac{\bar{v}_j+|\bar{v}_j|}{2\Delta x_i} + u^+_{i,j+1/2}\frac{-F_{i,j+1/2}+|F_{i,j+1/2}|}{2\Delta v} + u^-_{i,j+1/2}\frac{-F_{i,j+1/2}-|F_{i,j+1/2}|}{2\Delta v}$$
$$+ u^+_{i,j-1/2}\frac{F_{i,j-1/2}-|F_{i,j-1/2}|}{2\Delta v} + u^-_{i,j-1/2}\frac{F_{i,j-1/2}+|F_{i,j-1/2}|}{2\Delta v} + \frac{D}{\Delta v^2}(u^{n-1}_{i,j+1} - 2u^{n-1}_{i,j} + u^{n-1}_{i,j-1}).$$

The finite volume is constructed using (11) and (12) and

$$u^-_{i+1/2,j} = u_{i,j} + \frac{\Delta x_i}{2}(u_x)_{i,j},\ \ u^+_{i-1/2,j} = u_{i,j} - \frac{\Delta x_i}{2}(u_x)_{i,j},$$
$$u^-_{i,j+1/2} = u_{i,j} + \frac{\Delta v}{2}(u_v)_{i,j},\ \ u^+_{i,j-1/2} = u_{i,j} - \frac{\Delta v}{2}(u_v)_{i,j}.$$

Consequently we have

$$u^{n-1}_{i,j} = \frac{1}{4}\big(u^-_{i+1/2,j} + u^+_{i-1/2,j} + u^-_{i,j+1/2} + u^+_{i,j-1/2}\big).$$

For $0 \le w \le 1$ it can be re-written as

$$u^{n-1}_{i,j} = \frac{w}{4}\big(u^-_{i+1/2,j} + u^+_{i-1/2,j} + u^-_{i,j+1/2} + u^+_{i,j-1/2}\big) + (1-w)u^{n-1}_{i,j}. \tag{23}$$

Therefore, substituting (23) in the third term of the right-hand side of (23), we can write

$$\frac{d_{n-1}}{\Gamma(2-\alpha)}u^n_{i,j} = \frac{d_0}{\Gamma(2-\alpha)}u^0_{i,j} + \frac{1}{\Gamma(2-\alpha)}\sum_{p=1}^{n-2}(d_p-d_{p-1})u^p_{i,j}$$
$$+ \frac{w}{4\Gamma(2-\alpha)}(d_{n-1}-d_{n-2})\big(u^-_{i+1/2,j} + u^+_{i-1/2,j} + u^-_{i,j+1/2} + u^+_{i,j-1/2}\big)$$
$$+ \frac{1-w}{\Gamma(2-\alpha)}(d_{n-1}-d_{n-2})u^{n-1}_{i,j} + \frac{D}{\Delta v^2}(u^{n-1}_{i,j+1} - 2u^{n-1}_{i,j} + u^{n-1}_{i,j-1}) + u^+_{i+1/2,j}\frac{-\bar{v}_j+|\bar{v}_j|}{2\Delta x_i}$$
$$+ u^-_{i+1/2,j}\frac{-\bar{v}_j-|\bar{v}_j|}{2\Delta x_i} + u^+_{i-1/2,j}\frac{\bar{v}_j-|\bar{v}_j|}{2\Delta x_i} + u^-_{i-1/2,j}\frac{\bar{v}_j+|\bar{v}_j|}{2\Delta x_i} + u^+_{i,j+1/2}\frac{-F_{i,j+1/2}+|F_{i,j+1/2}|}{2\Delta v}$$
$$+ u^-_{i,j+1/2}\frac{-F_{i,j+1/2}-|F_{i,j+1/2}|}{2\Delta v} + u^+_{i,j-1/2}\frac{F_{i,j-1/2}-|F_{i,j-1/2}|}{2\Delta v} + u^-_{i,j-1/2}\frac{F_{i,j-1/2}+|F_{i,j-1/2}|}{2\Delta v}.$$

The only terms with negative coefficients are the coefficients of the diffusive term $-2u^{n-1}_{i,j}$ and the coefficients of $u^-_{i+1/2,j}$, $u^+_{i-1/2,j}$, $u^-_{i,j+1/2}$ and $u^+_{i,j-1/2}$. The reconstructed points are positive, by the way they were constructed as discussed in [5,16,23,24]. Therefore we reorganise the equality as

$$\frac{d_{n-1}}{\Gamma(2-\alpha)}u^n_{i,j} = \frac{d_0}{\Gamma(2-\alpha)}u^0_{i,j} + \frac{1}{\Gamma(2-\alpha)}\sum_{p=1}^{n-2}(d_p-d_{p-1})u^p_{i,j} + \frac{D}{\Delta v^2}(u^{n-1}_{i,j+1} + u^{n-1}_{i,j-1})$$
$$+ \left(\frac{1-w}{\Gamma(2-\alpha)}(d_{n-1}-d_{n-2}) - 2\frac{D}{\Delta v^2}\right)u^{n-1}_{i,j} + u^+_{i+1/2,j}\frac{-\bar{v}_j+|\bar{v}_j|}{2\Delta x_i} + u^-_{i-1/2,j}\frac{\bar{v}_j+|\bar{v}_j|}{2\Delta x_i}$$
$$+ u^+_{i,j+1/2}\frac{-F_{i,j+1/2}+|F_{i,j+1/2}|}{2\Delta v} + u^-_{i,j-1/2}\frac{F_{i,j-1/2}+|F_{i,j-1/2}|}{2\Delta v}$$
$$+ u^-_{i+1/2,j}\left(\frac{w}{4\Gamma(2-\alpha)}(d_{n-1}-d_{n-2}) + \frac{-\bar{v}_j-|\bar{v}_j|}{2\Delta x_i}\right) + u^+_{i-1/2,j}\left(\frac{w}{4\Gamma(2-\alpha)}(d_{n-1}-d_{n-2}) + \frac{\bar{v}_j-|\bar{v}_j|}{2\Delta x_i}\right)$$
$$+ u^-_{i,j+1/2}\left(\frac{w}{4\Gamma(2-\alpha)}(d_{n-1}-d_{n-2}) + \frac{-F_{i,j+1/2}-|F_{i,j+1/2}|}{2\Delta v}\right)$$
$$+ u^+_{i,j-1/2}\left(\frac{w}{4\Gamma(2-\alpha)}(d_{n-1}-d_{n-2}) + \frac{F_{i,j-1/2}-|F_{i,j-1/2}|}{2\Delta v}\right). \tag{24}$$

Since

$$\frac{1}{d_{n-1}-d_{n-2}}=\frac{2\Delta t_n^{\alpha}\Delta t_{n-1}}{\Delta t_n+\Delta t_{n-1}}\left(\frac{1}{2-2^{1-\alpha}(2\Delta t_n/(\Delta t_n+\Delta t_{n-1}))^{\alpha}}\right),$$

from condition (22) all the terms on the right-hand side of Eq. (24) are positive and the result follows. □

The constant w that appears in (22) in Theorem 1 can be chosen between 0 and 1. It is difficult to decide which value is the best choice since it will depend on the problem under consideration. A natural choice is to consider $w=1/2$.

Condition (22) is written for a non-uniform mesh in time. If the mesh is uniform in time, with time step Δt, it follows that

$$\Delta t^{\alpha}\leq\frac{2-2^{1-\alpha}}{\Gamma(2-\alpha)}\min\left\{\frac{\Delta v^2}{2D}(1-w),\frac{\Delta x_m}{v_M}\frac{w}{4},\frac{\Delta v}{F_M}\frac{w}{4}\right\}. \tag{25}$$

In the next theorem, the positivity preserving property is presented for the explicit method with the first-order approximation in phase space.

Theorem 2 (First-order explicit method)**.** *Consider the finite volume method (19) for $\tau=1$. Then the cell values $u_{i,j}(t_n)$ remain nonnegative provided the initial cell values are nonnegative and the following conditions are satisfied, for all $n\geq 1$,*

$$\frac{1}{\Delta t_{n+1/2}}\left(\frac{\Delta t_n^{\alpha}\Delta t_{n-1}\Gamma(2-\alpha)}{2-2^{1-\alpha}\left(\Delta t_n/\Delta t_{n+1/2}\right)^{\alpha}}\right)\leq\min\left\{\frac{\Delta v^2}{2D}(1-w),\frac{\Delta x_m}{v_M}\frac{w}{2},\frac{\Delta v}{F_M}\frac{w}{2}\right\}, \tag{26}$$

where $0<w<1$, $\Delta x_m=\min_i\Delta x_i$, $\Delta t_{n+1/2}=(\Delta t_n+\Delta t_{n-1})/2$, $v_M=\max|v|$ and $F_M=\max|F(x,v)|$.

Proof. The proof starts in the same way as the previous proof and we get (23). However now the intermediate values are given by

$$u^{-}_{i+1/2,j}=u^{n-1}_{i,j},\ u^{+}_{i-1/2,j}=u^{n-1}_{i,j},\ u^{-}_{i,j+1/2}=u^{n-1}_{i,j},\ u^{+}_{i,j-1/2}=u^{n-1}_{i,j}, \tag{27}$$

$$u^{+}_{i+1/2,j}=u^{n-1}_{i+1,j},\ u^{-}_{i-1/2,j}=u^{n-1}_{i-1,j},\ u^{-}_{i,j-1/2}=u^{n-1}_{i,j-1},\ u^{+}_{i,j+1/2}=u^{n-1}_{i,j+1}. \tag{28}$$

Proceeding similarly as in the previous theorem, by rearranging the terms and taking in consideration (27) and (28) we obtain

$$\begin{aligned}\frac{d_{n-1}}{\Gamma(2-\alpha)}u^{n}_{i,j}=&\frac{d_0}{\Gamma(2-\alpha)}u^{0}_{i,j}+\frac{1}{\Gamma(2-\alpha)}\sum_{p=1}^{n-2}(d_p-d_{p-1})u^{p}_{i,j}+\frac{D}{\Delta v^2}(u^{n-1}_{i,j+1}+u^{n-1}_{i,j-1})\\&+\left(\frac{1-w}{\Gamma(2-\alpha)}(d_{n-1}-d_{n-2})-2\frac{D}{\Delta v^2}\right)u^{n-1}_{i,j}+u^{n-1}_{i+1,j}\frac{-\bar v_j+|\bar v_j|}{2\Delta x_i}\\&+u^{n-1}_{i,j}\left(\frac{w}{2\Gamma(2-\alpha)}(d_{n-1}-d_{n-2})+\frac{-|\bar v_j|}{\Delta x_i}\right)\\&+u^{n-1}_{i-1,j}\frac{\bar v_j+|\bar v_j|}{2\Delta x_i}+u^{n-1}_{i,j+1}\frac{-F_{i,j+1/2}+|F_{i,j+1/2}|}{2\Delta v}+u^{n-1}_{i,j-1}\frac{F_{i,j-1/2}+|F_{i,j-1/2}|}{2\Delta v}\\&+u^{n-1}_{i,j}\left(\frac{w(d_{n-1}-d_{n-2})}{2\Gamma(2-\alpha)}+\frac{-F_{i,j+1/2}-|F_{i,j+1/2}|}{2\Delta v}+\frac{F_{i,j-1/2}-|F_{i,j-1/2}|}{2\Delta v}\right).\end{aligned} \tag{29}$$

Since $F_{i,j-1/2}\geq F_{i,j+1/2}$, if $F_{i,j-1/2}\geq 0$ and $F_{i,j+1/2}\geq 0$ then

$$-F_{i,j+1/2}-|F_{i,j+1/2}|+F_{i,j-1/2}-|F_{i,j-1/2}|=-2F_{i,j+1/2}. \tag{30}$$

If $F_{i,j-1/2}\geq 0$ and $F_{i,j+1/2}\leq 0$ then

$$-F_{i,j+1/2}-|F_{i,j+1/2}|+F_{i,j-1/2}-|F_{i,j-1/2}|=0, \tag{31}$$

and for $F_{i,j-1/2}\leq 0$ and $F_{i,j+1/2}\leq 0$

$$-F_{i,j+1/2}-|F_{i,j+1/2}|+F_{i,j-1/2}-|F_{i,j-1/2}|=2F_{i,j-1/2}. \tag{32}$$

Hence, condition (26) assure us that the terms on the right-hand side of (29) are positive and the result follows. □

For the first-order method, the positivity preserving property could have been obtained directly from Theorem 1 since the first-order method can be seen as a particular case of the general method described in Section 2.1. However, as shown in Theorem 2, an additional analysis allows to obtain a slightly less restrictive stability condition.

To prove the next theorems we will rely on the properties of M-matrices [3,15]. An invertible matrix $C=(c_{i,j})$ is called an M-matrix if $C^{-1}\geq 0$ and $c_{i,j}\leq 0$ for all $i\neq j$. A sufficient condition for a matrix $C=(c_{i,j})$ to be an M-matrix is $c_{i,j}\leq 0\,(i\neq j)$ and $c_{i,i}>\Sigma_{i\neq j}|c_{i,j}|$. Additionally, if $u\geq 0$ and $p=C^{-1}u$, then $p\geq 0$. This is the result that will be used in the next proofs.

The next result is related to the IMEX method. We have a second-order approximation in phase space for the fluxes and an implicit approach for the diffusive term to avoid the severe time restrictions for small D.

Theorem 3 (IMEX method)**.** *Consider the finite volume method (20). Then the cell values $u_{i,j}(t_n)$ remain nonnegative provided the initial cell values are nonnegative and the following conditions are satisfied, for all $n \geq 1$,*

$$\frac{1}{\Delta t_{n+1/2}}\left(\frac{\Delta t_n^{\alpha}\,\Delta t_{n-1}\Gamma(2-\alpha)}{2-2^{1-\alpha}\left(\Delta t_n/\Delta t_{n+1/2}\right)^{\alpha}}\right) \leq \min\left\{\frac{\Delta x_m}{\nu_M}\frac{1}{4}, \frac{\Delta \nu}{F_M}\frac{1}{4}\right\}, \tag{33}$$

where $\Delta x_m = \min_i \Delta x_i$, $\Delta t_{n+1/2} = (\Delta t_n + \Delta t_{n-1})/2$, $\nu_M = \max|\nu|$ and $F_M = \max|F(x,\nu)|$.

Proof. The part that involves the non-diffusive fluxes in Eq. (20) is similar to what we have discussed previously. The main difference is that the diffusive part is treated implicitly, that is, evaluated at time t_n. We consider the reconstructed points $u^{\pm}_{i\pm1/2,j}(t_{n-1})$ and $u^{\pm}_{i,j\pm1/2}(t_{n-1})$ and we omit the time step t_{n-1} for the sake of clarity. It follows

$$\begin{aligned}
\frac{d_{n-1}}{\Gamma(2-\alpha)}u^n_{i,j} = {} & \frac{d_0}{\Gamma(2-\alpha)}u^0_{i,j} - \frac{1}{\Gamma(2-\alpha)}\sum_{p=1}^{n-2}(d_{p-1}-d_p)u^p_{i,j} - \frac{1}{\Gamma(2-\alpha)}(d_{n-2}-d_{n-1})u^{n-1}_{i,j} + u^+_{i+1/2,j}\frac{-\bar{\nu}_j+|\bar{\nu}_j|}{2\Delta x_i} \\
& + u^-_{i+1/2,j}\frac{-\bar{\nu}_j-|\bar{\nu}_j|}{2\Delta x_i} + u^+_{i-1/2,j}\frac{\bar{\nu}_j-|\bar{\nu}_j|}{2\Delta x_i} + u^-_{i-1/2,j}\frac{\bar{\nu}_j+|\bar{\nu}_j|}{2\Delta x_i} + u^+_{i,j+1/2}\frac{-F_{i,j+1/2}+|F_{i,j+1/2}|}{2\Delta \nu} \\
& + u^-_{i,j+1/2}\frac{-F_{i,j+1/2}-|F_{i,j+1/2}|}{2\Delta \nu} + u^+_{i,j-1/2}\frac{F_{i,j-1/2}-|F_{i,j-1/2}|}{2\Delta \nu} \\
& + u^-_{i,j-1/2}\frac{F_{i,j-1/2}+|F_{i,j-1/2}|}{2\Delta \nu} + \frac{D}{\Delta \nu^2}(u^n_{i,j+1}-2u^n_{i,j}+u^n_{i,j-1}).
\end{aligned} \tag{34}$$

Using the fact that $4u^{n-1}_{i,j} = \left(u^-_{i+1/2,j} + u^+_{i-1/2,j} + u^-_{i,j+1/2} + u^+_{i,j-1/2}\right)$ the terms are rearranged in the following way

$$\begin{aligned}
& \frac{d_{n-1}}{\Gamma(2-\alpha)}u^n_{i,j} - \frac{D}{\Delta \nu^2}(u^n_{i,j+1}-2u^n_{i,j}+u^n_{i,j-1}) = \frac{d_0}{\Gamma(2-\alpha)}u^0_{i,j} + \frac{1}{\Gamma(2-\alpha)}\sum_{p=1}^{n-2}(d_p-d_{p-1})u^p_{i,j} + u^+_{i+1/2,j}\frac{-\bar{\nu}_j+|\bar{\nu}_j|}{2\Delta x_i} \\
& + u^-_{i-1/2,j}\frac{\bar{\nu}_j+|\bar{\nu}_j|}{2\Delta x_i} + u^-_{i+1/2,j}\left(\frac{d_{n-1}-d_{n-2}}{4\Gamma(2-\alpha)} + \frac{-\bar{\nu}_j-|\bar{\nu}_j|}{2\Delta x_i}\right) + u^+_{i-1/2,j}\left(\frac{d_{n-1}-d_{n-2}}{4\Gamma(2-\alpha)} + \frac{\bar{\nu}_j-|\bar{\nu}_j|}{2\Delta x_i}\right) \\
& + u^+_{i,j+1/2}\frac{-F_{i,j+1/2}+|F_{i,j+1/2}|}{2\Delta \nu} + u^-_{i,j-1/2}\frac{F_{i,j-1/2}+|F_{i,j-1/2}|}{2\Delta \nu} + u^-_{i,j+1/2}\left(\frac{d_{n-1}-d_{n-2}}{4\Gamma(2-\alpha)} + \frac{-F_{i,j+1/2}-|F_{i,j+1/2}|}{2\Delta \nu}\right) \\
& + u^+_{i,j-1/2}\left(\frac{d_{n-1}-d_{n-2}}{4\Gamma(2-\alpha)} + \frac{F_{i,j-1/2}-|F_{i,j-1/2}|}{2\Delta \nu}\right).
\end{aligned} \tag{35}$$

The vector form of the finite volume scheme is

$$\left(\frac{\Delta t_n^{-\alpha}}{\Gamma(2-\alpha)}\mathbf{I}+\mathbf{B}\right)\mathbf{U}^n = \frac{d_0}{\Gamma(2-\alpha)}\mathbf{U}^0 + \frac{1}{\Gamma(2-\alpha)}\sum_{p=1}^{n-2}(d_p-d_{p-1})\mathbf{U}^p + \mathbf{L}(\mathbf{U}^+_{x+},\mathbf{U}^-_{x+},\mathbf{U}^+_{x-},\mathbf{U}^-_{x-},\mathbf{U}^+_{\nu+},\mathbf{U}^-_{\nu+},\mathbf{U}^+_{\nu-},\mathbf{U}^-_{\nu-}),$$

where $\mathbf{U}^k$ is a vector containing the cell averages $u^k_{i,j}$, $\mathbf{B}$ is the tridiagonal matrix associated to the diffusive part, $\mathbf{U}^{\pm}_{x\pm}, \mathbf{U}^{\pm}_{\nu\pm}$ are vectors containing the reconstructed point values and $\mathbf{L}$ is a vector, with each element being the linear combination of the corresponding point values in $\mathbf{U}^{\pm}_{x\pm}, \mathbf{U}^{\pm}_{\nu\pm}$.

The vector form can also be written as

$$\mathbf{M}\mathbf{U}^n = \Delta t_n^{\alpha} d_0 \mathbf{U}^0 + \Delta t_n^{\alpha}\sum_{p=1}^{n-2}(d_p-d_{p-1})\mathbf{U}^p + \Delta t_n^{\alpha}\Gamma(2-\alpha)\mathbf{L},$$

for $\mathbf{M} = \mathbf{I} + \Delta t_n^{\alpha}\Gamma(2-\alpha)\mathbf{B}$. It follows that

$$\mathbf{U}^n = \mathbf{M}^{-1}\left(\Delta t_n^{\alpha} d_0 \mathbf{U}^0 + \Delta t_n^{\alpha}\sum_{p=1}^{n-2}(d_p-d_{p-1})\mathbf{U}^p + \Delta t_n^{\alpha}\Gamma(2-\alpha)\mathbf{L}\right). \tag{36}$$

The main diagonal of $\mathbf{B}$ is $2D/\Delta\nu^2$ and there are two diagonals with the values $-D/\Delta\nu^2$ and therefore $\mathbf{M} = \mathbf{I} + \Delta t_n^{\alpha}\Gamma(2-\alpha)\mathbf{B}$ is an M-matrix. The right-hand side is positive if the condition (33) is verified. Consequently, it is known [3,15] that all the components of the linear system (36) are also non-negative and the proof is complete. □

Since we have quite restrictive conditions for small values of α there is the need of using an implicit scheme. In this case the implicit has a significant advantage over the explicit for values α near zero.

Theorem 4 (Implicit method)**.** *Consider the finite volume method (21). Then the cell values $u_{i,j}(t_n)$ remain nonnegative provided the initial cell values are nonnegative and that*

$$\Delta t_n^{\alpha} \leq \frac{1}{\gamma\,\Gamma(2-\alpha)}. \tag{37}$$

Proof. Let us go back to (23) and now taking in consideration that

$$u^{+}_{i+1/2,j} = u^{n}_{i+1,j}, \quad u^{-}_{i+1/2,j} = u^{n}_{i,j}, \quad u^{+}_{i-1/2,j} = u^{n}_{i,j}, \quad u^{-}_{i-1/2,j} = u^{n}_{i-1,j},$$

and that

$$u^{+}_{i,j+1/2} = u^{n}_{i,j+1}, \quad u^{-}_{i,j+1/2} = u^{n}_{i,j}, \quad u^{+}_{i,j-1/2} = u^{n}_{i,j}, \quad u^{-}_{i,j-1/2} = u^{n}_{i,j-1},$$

we obtain

$$\begin{aligned}\frac{d_{n-1}}{\Gamma(2-\alpha)}u^{n}_{i,j} = {} & \frac{d_0}{\Gamma(2-\alpha)}u^{0}_{i,j} + \frac{1}{\Gamma(2-\alpha)}\sum_{p=1}^{n-1}(d_p - d_{p-1})u^{p}_{i,j} + u^{n}_{i+1,j}\frac{-\bar{v}_j + |\bar{v}_j|}{2\Delta x_i} + u^{n}_{i,j}\frac{-\bar{v}_j - |\bar{v}_j|}{2\Delta x_i} + u^{n}_{i,j}\frac{\bar{v}_j - |\bar{v}_j|}{2\Delta x_i} \\ & + u^{n}_{i-1,j}\frac{\bar{v}_j + |\bar{v}_j|}{2\Delta x_i} + u^{n}_{i,j+1}\frac{-F_{i,j+1/2} + |F_{i,j+1/2}|}{2\Delta v} + u^{n}_{i,j}\frac{-F_{i,j+1/2} - |F_{i,j+1/2}|}{2\Delta v} \\ & + u^{n}_{i,j}\frac{F_{i,j-1/2} - |F_{i,j-1/2}|}{2\Delta v} + u^{n}_{i,j-1}\frac{F_{i,j-1/2} + |F_{i,j-1/2}|}{2\Delta v} + \frac{D}{\Delta v^2}(u^{n}_{i,j+1} - 2u^{n}_{i,j} + u^{n}_{i,j-1}).\end{aligned} \tag{38}$$

Rearranging the terms we can write

$$\begin{aligned}&\frac{d_{n-1}}{\Gamma(2-\alpha)}u^{n}_{i,j} + \frac{D}{\Delta v^2}(-u^{n}_{i,j+1} + 2u^{n}_{i,j} - u^{n}_{i,j-1}) + a_{ij}u^{n}_{i+1,j} + b_{ij}u^{n}_{i,j} + c_{ij}u^{n}_{i-1,j} \\ &+ d_{ij}u^{n}_{i,j+1} + e_{ij}u^{n}_{i,j-1} = \frac{d_0}{\Gamma(2-\alpha)}u^{0}_{i,j} + \frac{1}{\Gamma(2-\alpha)}\sum_{p=1}^{n-1}(d_p - d_{p-1})u^{p}_{i,j},\end{aligned} \tag{39}$$

where

$$\begin{aligned}a_{ij} &= -\frac{-\bar{v}_j + |\bar{v}_j|}{2\Delta x_i}, \quad c_{ij} = -\frac{\bar{v}_j + |\bar{v}_j|}{2\Delta x_i}, \\ b_{ij} &= \frac{|\bar{v}_j|}{\Delta x_i} + \frac{F_{i,j+1/2} + |F_{i,j+1/2}| - F_{i,j-1/2} + |F_{i,j-1/2}|}{2\Delta v}, \\ d_{ij} &= -\frac{-F_{i,j+1/2} + |F_{i,j+1/2}|}{2\Delta v}, \quad e_{ij} = -\frac{F_{i,j-1/2} + |F_{i,j-1/2}|}{2\Delta v}.\end{aligned}$$

The finite volume scheme in the vector form is

$$\left(\frac{\Delta t_n^{-\alpha}}{\Gamma(2-\alpha)}\mathbf{I} + \mathbf{A} + \mathbf{B}\right)\mathbf{U}^{n} = \frac{d_0}{\Gamma(2-\alpha)}\mathbf{U}^{0} + \frac{1}{\Gamma(2-\alpha)}\sum_{p=1}^{n-1}(d_p - d_{p-1})\mathbf{U}^{p},$$

where $\mathbf{B}$ is the same matrix as the matrix $\mathbf{B}$ in the previous theorem and $\mathbf{A}$ is the matrix that contains the values a_{ij}, b_{ij}, c_{ij}, d_{ij} and e_{ij} related to the fluxes.

The rest of the proof consists in showing that if condition (37) is verified then the matrix $\frac{\Delta t_n^{-\alpha}}{\Gamma(2-\alpha)}\mathbf{I} + \mathbf{A} + \mathbf{B}$ is an M-matrix. The elements in the main diagonal are non-negative since

$$\frac{\Delta t_n^{-\alpha}}{\Gamma(2-\alpha)} + \frac{2D}{\Delta v^2} + b_{ij} \geq 0,$$

where b_{ij} is positive because we have (30)–(32). The matrix elements located in the other four diagonals are non-positive since

$$a_{ij} \leq 0, \quad c_{ij} \leq 0, \quad d_{ij} \leq 0, \quad e_{ij} \leq 0.$$

It is now sufficient for $\frac{\Delta t_n^{-\alpha}}{\Gamma(2-\alpha)}\mathbf{I} + \mathbf{A} + \mathbf{B}$ to be an M-matrix to verify that it is also true that

$$\frac{\Delta t_n^{-\alpha}}{\Gamma(2-\alpha)} + \frac{2D}{\Delta v^2} + b_{ij} \geq |a_{ij}| + |c_{ij}| + |d_{ij}| + |e_{ij}| + \frac{D}{\Delta v^2} + \frac{D}{\Delta v^2}. \tag{40}$$

Since

$$|a_{ij}| + |c_{ij}| = \frac{|\bar{v}_j|}{\Delta x_i} \quad \text{and} \quad |d_{ij}| + |e_{ij}| = \frac{-F_{i,j+1/2} + |F_{i,j+1/2}| + F_{i,j-1/2} + |F_{i,j-1/2}|}{2\Delta v},$$

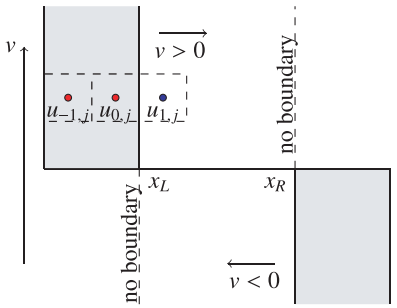

Fig. 2. Absorbing boundary conditions. The fictitious points needed are in the grey zone, that represent the part where we have a boundary. On the other part of the domain, respectively, there is no boundary.

the inequality (40) is equivalent to

$$\frac{\Delta t_n^{-\alpha}}{\Gamma(2-\alpha)} + \frac{F_{i,j+1/2} + |F_{i,j+1/2}| - F_{i,j-1/2} + |F_{i,j-1/2}|}{2\Delta v} \geq \frac{-F_{i,j+1/2} + |F_{i,j+1/2}| + F_{i,j-1/2} + |F_{i,j-1/2}|}{2\Delta v}. \tag{41}$$

It follows that (41) can be rewritten as

$$\frac{\Delta t_n^{-\alpha}}{\Gamma(2-\alpha)} \geq -\frac{F_{i,j+1/2} - F_{i,j-1/2}}{\Delta v}. \tag{42}$$

We have that $F_{i,j+1/2} - F_{i,j-1/2} = -\gamma(\tilde{v}_{j+1/2} - \tilde{v}_{j-1/2})$ and therefore

$$\frac{\Delta t_n^{-\alpha}}{\Gamma(2-\alpha)} \geq \gamma\left(\frac{\tilde{v}_j + \Delta v/2 - \tilde{v}_j + \Delta v/2}{\Delta v}\right) = \gamma. \tag{43}$$

This is the same as condition (37) and the proof is complete. □

The condition presented in the previous theorem is not a stability restriction since it does not impose a dependence between Δt and Δv or Δx_i. Restrictions for positivity preserving implicit methods appear in other works, such as, for differential equations of integer order [14]. It is also reported that for implicit methods, of order higher than one in time, strong stability conditions as the ones observed for explicit methods can be expected, which is not the case in our context.

In our case this restriction depends on the physical parameter $\gamma > 0$, that is, the friction parameter. In particular, this parameter is related with the parameters D and T_p through Eq. (5). One can ask what are the γ values in some physical situations. Usually when the values of the friction parameter are very high we obtain the Fokker-Planck equation derived from the Langevin equation. The Klein-Kramers equation is derived assuming the friction parameter is not very large. Therefore the condition is even less restrictive by taking into consideration that from the physical point of view large values of γ should not be considered. Large values of γ correspond to either large diffusion D or low temperature T_p (see Eq. (5)).

4. Formulation of the boundary conditions and the positivity preserving property

Additionally to the study of the open domain problem, the case of having a bounded domain in the spatial direction is discussed and absorbing boundary conditions or reflecting boundary conditions are considered. To implement these boundary conditions the finite volume schemes need to be reformulated for the cells near the boundary. In particular, we describe how to implement the implicit method and the second-order IMEX method in the presence of boundary conditions. The other methods considered in Section 2 can be similarly modified.

4.1. Absorbing boundary conditions

The absorbing boundary conditions are, for all $t > 0$, given by

$$u(x_L, v, t) = 0,\ v > 0, \quad \text{and} \quad u(x_R, v, t) = 0,\ v < 0. \tag{44}$$

If the first-order approximation is used in the full domain, as it happens in the case of the implicit method, the implementation of the absorbing boundary conditions is straightforward. However, for the second-order spatial approximation that appears in the case of the IMEX method, we do not have the necessary cells available near the boundary.

For the IMEX method with the second-order approximation, we proceed, near the boundary, in the following way. At x_L for $v > 0$ the computational domain is extended as needed and set $u_{i,j} = 0$ at the corresponding extra cells, as illustrated in Fig. 2. We proceed similarly near x_R for $v < 0$.

In the parts of the domain where there is no boundary in x, the first-order scheme is considered since no extra information outside the domain is needed. For $v > 0$ a right boundary is not needed and for $v < 0$ a left boundary is not needed

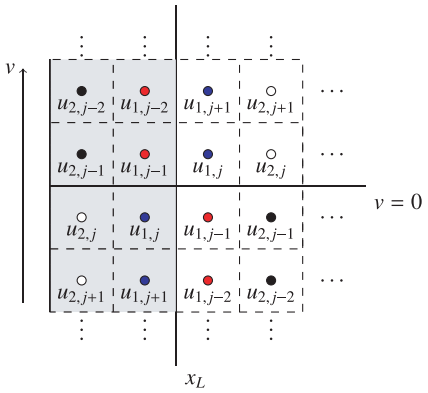

Fig. 3. Reflecting boundary conditions represented at $x = x_L$. For $x = x_R$ we have a similar procedure. The fictitious points needed are in the grey zone and the values they take are assigned. The symmetry is highlighted by colors.

as illustrated in Fig. 2. If we use the first-order approximation near these parts, this means that in (14) the term involving the function f_u^x is approximated as

$$\frac{f_u^x(\bar{x}_{i+1/2}, \bar{v}_j, t) - f_u^x(\bar{x}_{i-1/2}, \bar{v}_j, t)}{\Delta x_i} \simeq \begin{cases} \bar{v}_j \dfrac{u_{i,j} - u_{i-1,j}}{\Delta x_i}, & \bar{v}_j > 0 \\ \bar{v}_j \dfrac{u_{i+1,j} - u_{i,j}}{\Delta x_i} & \bar{v}_j < 0, \end{cases}$$

where the values of f_u^x are according to Remark 1. This is done for the first and last cells, that is, $u_{i,j}, i = N_x - 1$, for $v > 0$ and $i = 1$ when $v < 0$.

Regarding the properties of the finite volume method with the absorbing boundary conditions, similar conditions are obtained for the non-negativity of the numerical solutions. For the implicit method we can derive the same result as the one stated in Theorem 4 since the boundary conditions are non-negative and no changes where done in the numerical approximations. For the IMEX method with the second-order approximation a first-order approximation was imposed near the boundary and this slightly changes the method. For this method the final stability condition consists on the intersection of the condition obtained for the second-order finite volume method with the condition obtained for the first-order finite volume method. Considering that the first-order approximation imposes less restrictive conditions regarding non-negativity, given in Theorem 2, we obtain the same condition as the one stated in Theorem 1.

Since the assumption of absorbing boundary conditions requires the use of the first-order approximation, one may ask if the overall accuracy of the method is influenced by this change. In the section of the numerical tests, it will be observed that this happens and that to recover the second-order accuracy a non-uniform mesh can be used, which is more refined near the boundary.

4.2. Reflecting boundary conditions

Other type of boundary conditions frequently associated with the Klein-Kramers equation are the following reflecting boundary conditions

$$u(x_L, v, t) = u(x_L, -v, t) \quad \text{and} \quad u(x_R, v, t) = u(x_R, -v, t). \tag{45}$$

To implement (45) we first extend the finite volume grid, near $x = x_L$, by setting

$$\bar{x}_0 = \bar{x}_1 - \Delta x_1, \quad \bar{x}_{-1} = \bar{x}_0 - \frac{\Delta x_1 + \Delta x_2}{2}.$$

Similarly, near $x = x_R$ we set

$$\bar{x}_{N_x} = \bar{x}_{N_x-1} + \Delta x_{Nx}, \quad \bar{x}_{N_x+1} = \bar{x}_{N_x} + \frac{\Delta x_{N_x} + \Delta x_{N_x-1}}{2}.$$

To decide which values the fictitious cells should have we take into consideration the symmetry imposed by the reflective boundary conditions, that is, the fictitious finite volume cells are chosen inspired on the reflective property (45). This is illustrated in Fig. 3. In general, we define, near $x = x_L$,

$$u_{0,j} = u_{1,N_v^*-j+1}, \quad j = 1, \ldots, N_v^*, \quad u_{-1,j} = u_{2,N_v^*-j+1}, \quad j = 1, \ldots, N_v^*.$$

Similarly, near $x = x_R$, we take

$$u_{N_x,j} = u_{N_x-1,N_v^*-j+1}, j = 1, \ldots, N_v^*; \; u_{N_x+1,j} = u_{N_x-2,N_v^*-j+1}, j = 1, \ldots, N_v^*.$$

Here, $N_v^* = N_v - 1$ and we assume that N_v^* is an even number and also that $v_L = -v_R$.

Regarding the properties of the finite volume schemes we discuss the implicit method and the IMEX method as done previously for the absorbing boundary conditions. For the implicit method, from (39), we have, for $i = 1$,

$$\frac{d_{n-1}}{\Gamma(2-\alpha)}u_{1,j}^n + \frac{D}{\Delta v^2}(-u_{1,j+1}^n + 2u_{1,j}^n - u_{1,j-1}^n) + a_{1j}u_{2,j}^n + b_{ij}u_{1,j}^n + c_{1j}u_{0,j}^n + d_{1j}u_{1,j+1}^n + e_{1j}u_{1,j-1}^n$$
$$= \frac{d_0}{\Gamma(2-\alpha)}u_{1,j}^0 + \frac{1}{\Gamma(2-\alpha)}\sum_{p=1}^{n-1}(d_p - d_{p-1})u_{1,j}^p.$$

We have a fictitious point $u_{0,j}^n$ and we take $u_{0,j}^n = u_{1,N_v^*-j+1}^n$. Since the new element is not equal to an element in the diagonal of the matrix represented in the proof of Theorem 4, and the coefficient c_{1j} has the same sign as all the elements out of the diagonal, we can follow the same steps of the proof of Theorem 4 and conclude that Theorem 4 remains valid for the case when reflecting boundary conditions are assumed. A similar justification can be given to the approximations near the other side of the boundary.

For the IMEX method, from (34), for $i = 1$, it follows

$$\frac{d_{n-1}}{\Gamma(2-\alpha)}u_{1,j}^n = \frac{d_0}{\Gamma(2-\alpha)}u_{1,j}^0 - \frac{1}{\Gamma(2-\alpha)}\sum_{p=1}^{n-1}(d_{p-1} - d_p)u_{1,j}^p + u_{1+1/2,j}^+\frac{-\bar{v}_j + |\bar{v}_j|}{2\Delta x_i} + u_{1+1/2,j}^-\frac{-\bar{v}_j - |\bar{v}_j|}{2\Delta x_i}$$
$$+ u_{1-1/2,j}^+\frac{\bar{v}_j - |\bar{v}_j|}{2\Delta x_i} + u_{1-1/2,j}^-\frac{\bar{v}_j + |\bar{v}_j|}{2\Delta x_i} + u_{1,j+1/2}^+\frac{-F_{i,j+1/2} + |F_{i,j+1/2}|}{2\Delta v} + u_{1,j+1/2}^-\frac{-F_{i,j+1/2} - |F_{i,j+1/2}|}{2\Delta v}$$
$$+ u_{1,j-1/2}^+\frac{F_{i,j-1/2} - |F_{i,j-1/2}|}{2\Delta v} + u_{1,j-1/2}^-\frac{F_{i,j-1/2} + |F_{i,j-1/2}|}{2\Delta v} + \frac{D}{\Delta v^2}(u_{1,j+1}^n - 2u_{1,j}^n + u_{1,j-1}^n).$$

The main point, in this case, is that the positivity of the solution is based on the positivity of the reconstructed values that is guaranteed by the minmod limiter (13). The minmod limiter also guarantees the positivity of the reconstructed values when the relations illustrated in Fig. 3 are used. Therefore the positivity is guaranteed for the reflecting boundary conditions.

5. Numerical tests

In this section several numerical tests are presented in order to observe the convergence rates of the implicit method (21) and the IMEX method (20). We start to discuss the problem with homogeneous boundary conditions, since it simulates a problem defined in an open domain. In Section 5.2 it is discussed how the presence of absorbing boundary conditions affects the performance of the finite volume schemes. The same is done in Section 5.3 for the reflective boundary conditions. In Section 5.4 the convergence rates are discussed when the time is refined. Finally, in the last subsection numerical solutions for different force fields are presented and the performance of a positivity preserving method is compared with the performance of an existing method in literature.

5.1. Homogeneous boundary conditions

The convergence results for the implicit method (21) and the IMEX method (20) are presented and it is shown that for the implicit method we obtain first-order convergence and for the IMEX method we have second-order convergence in phase space. The sharpness of the positivity preserving condition (stability condition) derived in Section 3 is also discussed.

In order to illustrate the convergence rate of the numerical methods we consider a problem defined in the (x, v)-domain $[0, 2] \times [0, 2]$ and $t \in [0, T]$, with $T = 1$. Homogeneous boundary conditions are assumed and the parameters in Eq. (6) are defined as $D = 1$, $\gamma = 1$ and $F(x, v) = x^2 - v$. A source term is included on the right-hand side of the equation in order to have access to the exact solution.

We define the initial condition and the source term, such that, the exact solution of the problem, shown in Fig. 4, is given by $u(x, v, t) = t^2v^4x^4(2-x)^4(2-v)^4$. The source term can be determined by substituting this exact solution in Eq. (6).

In the next tables we display the errors between the exact solution and the numerical solution given by

$$E_{N_x,N_v}^M = \max_{n=1,\ldots,M}\left(\max_i \Delta x_i \Delta v \sum_{i=1}^{N_x-1}\sum_{j=1}^{N_v-1}(u_{i,j}^n - u(x_i, v_j, t_n))^2\right)^{1/2}. \tag{46}$$

The rate of convergence is measured by

$$\text{Rate} = \frac{\log(E_{N_x,N_v}^M) - \log(E_{\tilde{N}_x,\tilde{N}_v}^M)}{\log(\min\{\tilde{N}_x, \tilde{N}_v\}) - \log(\min\{N_x, N_v\})}, \tag{47}$$

for $\min\{N_x, N_v\}) < \min\{\tilde{N}_x, \tilde{N}_v\}$ and where $N_x, \tilde{N}_x$ and $N_v, \tilde{N}_v$ are the number of space and phase grid points respectively and they are associated with two meshes that keep the same number of grid points in time, M.

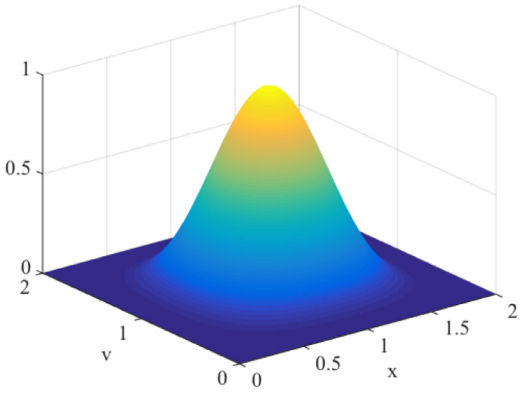

Fig. 4. Surface of the exact solution for Eq. (6) with a source term, initial condition zero and homogeneous boundary conditions when the final time is $T = 1$ and $D = 1$, $\gamma = 1$, $F(x, v) = x^2 - v$.

Table 1
Implicit method: first-order in phase space and time step $\Delta t = 0.01$. The error E_1 is obtained for a uniform mesh with $\Delta x = \Delta v = 0.1$. The error E_2 is obtained with the previous mesh divided by two, that is, $\Delta x = \Delta v = 0.05$.

α	E_1	CPU time	E_2	CPU time	Rate
0.9	3.7408e-02	6.0901e-01	1.9390e-02	1.0915e+00	9.4806e-01
0.7	3.9486e-02	4.2027e-01	2.0669e-02	9.2138e-01	9.3388e-01
0.5	4.1148e-02	4.4147e-01	2.1580e-02	9.8165e-01	9.3113e-01
0.3	4.2646e-02	4.0469e-01	2.2362e-02	9.6498e-01	9.3139e-01
0.1	4.4052e-02	3.9889e-01	2.3084e-02	9.7079e-01	9.3231e-01

Table 2
IMEX method: second-order in phase space. To determine E_1 and E_2 the mesh sizes Δx and Δv are the same as in Table 1.

α	E_1	Δt	CPU time	E_2	Δt	CPU time	Rate
0.9	5.1459e-03	3.6605e-03	1.7889e+00	1.2090e-03	1.6473e-03	3.6158e+00	2.0896
0.7	5.3186e-03	6.1194e-04	6.8780e+00	1.2370e-03	2.1921e-04	6.0870e+01	2.1043
0.5	5.4583e-03	1.8886e-05	2.8377e+03	1.2904e-03	4.4868e-06	9.2461e+04	2.0806

Table 3
IMEX method: second-order in phase space. The mesh sizes Δx and Δv are chosen as in Table 1. The choice of the time step does not obey the positivity preserving condition derived in Section 3. On the first column, Δt^* stands for the time step considered in Table 2 and $2\Delta t^*$, $20\Delta t^*$, $260\Delta t^*$ is the actual value considered for Δt in the third and fifth column.

α	E_1	Δt	CPU time	E_2	Δt	CPU time	Rate
($2\Delta t^*$) 0.9	5.6258e-03	7.3210e-03	1.1626e+00	1.6738e-03	3.2945e-03	1.7442e+00	1.7490
($20\Delta t^*$) 0.7	7.1498e-03	1.2239e-02	5.8045e-01	2.1482e-03	4.3842e-03	1.3037e+00	1.7348
($260\Delta t^*$) 0.5	5.4514e-03	4.9103e-03	7.6518e-01	1.5944e-03	1.1666e-03	4.9680e+00	1.7736

The information of the CPU time in seconds is included in all the tables of this subsection. The proposed numerical methods were implemented in MATLAB R2018b on a computer with a 3.4 GHz IntelCore i7 processor and 16 GB of RAM.

In Table 1 the results for the implicit scheme are shown and the first-order convergence is observed. The error defined according to (46) and denoted by E_1 is displayed for a uniform mesh in phase space with $\Delta x = \Delta v = 0.1$ and for $\Delta t = 0.01$. To determine the second error, denoted by E_2, the previous mesh is divided by two, that is, $\Delta x = \Delta v = 0.05$.

The results for the IMEX method are shown in Table 2 and the second-order convergence in phase space is achieved. The time step is displayed in Table 2 since now we have a conditionally stable numerical method and the time step depends on the phase step, space step and also on the value of α. The error values E_1 and E_2 are for the same mesh sizes as the ones considered in Table 1.

In Table 3, it is shown how the violation of the stability condition given by the positivity preserving property in Section 3, for the IMEX method, affects the results. The numerical method does not seem to blow up for the chosen values of the phase, space and time steps but the convergence rate is not two anymore. For larger values of Δt the scheme stops to converge.

The CPU times shown in Table 1, for the implicit method, and shown in Table 2, for the IMEX method, highlights the advantage of using an implicit method, in particular for smaller values of α. This is a consequence of the stability condition

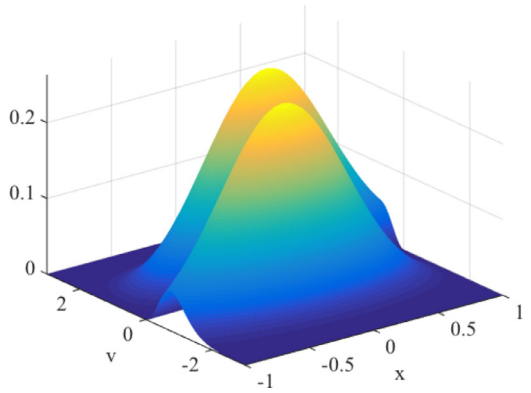

Fig. 5. Surface of the exact solution for Eq. (6) with a source term, initial condition zero and absorbing boundary conditions when the final time is $T = 1$ and $D = 1,\ \gamma = 1,\ F(x, v) = x^2 - v$.

Table 4
Absorbing boundary conditions and implicit numerical method: numerical results for $\Delta t = 0.01$. The error E_1 is obtained for a uniform mesh in x and v, with $\Delta x = \Delta v = 0.1$. The error E_2 is obtained with the previous mesh divided by two, that is, $\Delta x = \Delta v = 0.05$.

α	E_1	E_2	Rate
0.9	1.3023e-02	6.5289e-03	9.9617e-01
0.7	1.4731e-02	7.6333e-03	9.4852e-01
0.5	1.6104e-02	8.4240e-03	9.3481e-01
0.3	1.7379e-02	9.1124e-03	9.3141e-01
0.1	1.8637e-02	9.7772e-03	9.3065e-01

Table 5
Absorbing boundary conditions for the IMEX method, second-order in phase space with first-order approximation in space near the boundary, that is, at $x = -1,\ v \leq 0$ and $x = 1,\ v \geq 0$. To determine E_1 and E_2 the mesh sizes are the same as in Table 4.

α	E_1	Δt	E_2	Δt	Rate
0.9	3.4311e-03	3.5564e-03	1.2952e-03	1.6241e-03	1.4055
0.7	3.4526e-03	5.8966e-04	1.2759e-03	2.1526e-04	1.4362

required by the IMEX method that forces the time step to be small. Once the small step is less restrictive the CPU time is greatly diminished as can be seen in Table 3.

5.2. Absorbing boundary conditions

In this section, we assume absorbing boundary conditions in the spatial direction. The numerical tests have the purpose of clarifying the effect of considering a lower order method near the boundary, as a result of having boundaries, and also to show the advantage of having a non-uniform mesh in space. To recover the second-order accuracy, it will be enough to divide the nearest cell to the boundary in two cells and to choose the size of the closest new cell to the boundary as Δx^2, where Δx was the previous size.

Consider the Klein-Kramers equation with absorbing boundary conditions, defined in the (x, v)-domain $[-1, 1] \times [-3, 3]$ and $t \in [0, T]$, with $T = 1$. For the variables in Eq. (6), we consider $D = 1,\ \gamma = 1$ and $F(x, v) = x^2 - v$. A source term is included on the right-hand side of the equation, in order to be able to get an exact solution. The exact solution is shown in Fig. 5 and is given by $u(x, v, t) = t^2\left(1 - e^{-(x|v|v+v^2)}\right)e^{-v^2}e^{-2x^2}$.

The errors are measured according to (46) as in the previous subsection and the rates of convergence are computed also according to (47). The mesh sizes in the (x, v) phase space are the same as the ones considered in Section 5.1.

In Table 4, the results for the implicit method are presented and the expected first-order convergence rate is obtained. In Table 5, the results for the second-order IMEX method are displayed and because we are in the presence of boundaries, a first-order approximation in space is used near the boundary as described previously in Section 4. We see that using a lower order approximation near the boundary culminates in a lost of the overall second-order accuracy. The last test shown in Table 6 consists of using the IMEX method with the first-order accuracy at the boundary as in the test shown in Table 5, but now with a non-uniform mesh. It intends to illustrate that we can recover the second-order accuracy by

Table 6
Absorbing boundary conditions for the IMEX method: second-order in phase space with first-order approximation in space near the boundary. First-order approximation at $x = -1,\ v \leq 0$ and $x = 1,\ v \geq 0$. Refined mesh near the boundary, that is, the first space step $\Delta x = 0.1$ is now replaced by $\Delta x_1 = 0.02$ and $\Delta x_2 = 0.08$.

α	E_1	Δt	E_2	Δt	Rate
0.9	1.5984e-03	3.7577e-04	3.9975e-04	1.7234e-04	1.9995
0.7	1.6463e-03	3.2782e-05	4.1975e-04	1.2032e-05	1.9716

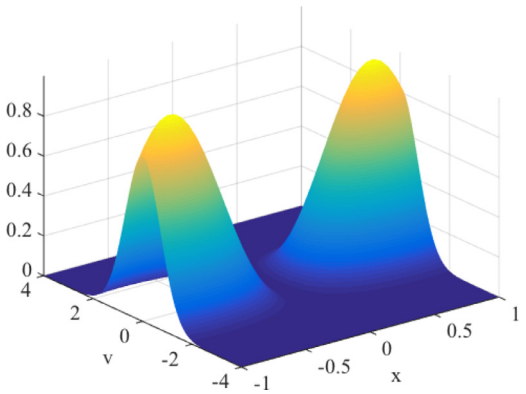

Fig. 6. Surface of the exact solution for Eq. (6) with a source term, initial condition zero and reflecting boundary conditions when the final time is $T = 1$ and $D = 1,\ \gamma = 1,\ F(x, v) = x^2 - v$.

Table 7
Reflecting boundary conditions and implicit numerical method: numerical results for $\Delta t = 0.01$. The error E_1, obtained for a uniform mesh in x, with $\Delta x = \Delta v = 0.1$. The error E_2 obtained with the previous mesh divided by two, that is, $\Delta x = \Delta v = 0.05$.

α	E_1	E_2	Rate
0.9	5.1455e-02	2.7102e-02	9.2492e-01
0.7	5.7428e-02	3.0634e-02	9.0665e-01
0.5	6.2243e-02	3.3334e-02	9.0092e-01
0.3	6.6529e-02	3.5637e-02	9.0058e-01
0.1	7.0552e-02	3.7766e-02	9.0162e-01

refining the mesh near the boundary points. In particular, for the cells near the left boundary, it was considered $\Delta x_1 = 0.02$ and $\Delta x_2 = 0.08$ to replace the nearest cell to the boundary of size $\Delta x = 0.1$. In the right part of the domain we have proceeded similarly by doing $\Delta x_{N_x - 1} = 0.02,\ \Delta x_{N_x} = 0.08$ to refine $\Delta x = 0.1$.

5.3. Reflecting boundary conditions

In this section, numerical tests are presented for the problem with reflecting boundary conditions in space. As we have seen a consequence of using a second-order scheme with this type of boundaries is the need of using fictitious points. Therefore, the effect of using fictitious points is shown and also the advantage of having a non-uniform mesh in space. To keep the second-order accuracy it will be enough to divide the nearest cell to the boundary in three cells and to choose the size of the two closest new cells to the boundary as Δx^2, where Δx was the previous size.

Consider the Klein-Kramers equation with reflecting boundary conditions, defined in the (x, v)-domain $[-1, 1] \times [-4, 4]$ and $t \in [0, T]$, with $T = 1$. For the variables in Eq. (6), we consider $D = 1,\ \gamma = 1$ and $F(x, v) = x^2 - v$. A source term is assumed on the right-hand side of the equation, in order to be able to get an exact solution. The exact solution is shown in Fig. 6 and is given by $u(x, v, t) = t^2 \sin^2(2x) e^{-v^2}$.

As previously, the errors and the rates are measured according to (46) and (47) respectively.

We have considered the same mesh in the (x, v) phase space as in Section 5.1 and Section 5.2. In Table 7, the first-order convergence rate can be observed for the implicit method. In Table 8, the results for the second-order IMEX method are presented. To deal with the fictitious volume cells needed to compute the cell near the boundary, a new formulation of the finite volume scheme was done as explained in Section 4. The idea was to take in consideration the symmetry imposed by the reflective boundary conditions. However, the overall second-order accuracy is lost, as shown in Table 8.

Table 8
Second-order in space and first-order IMEX in time. To determine E_1 and E_2 the mesh sizes considered are the same as in Table 7.

α	E_1	Δt	E_2	Δt	Rate
0.9	1.3366e-02	3.5564e-03	5.7585e-03	1.6241e-03	1.2147
0.7	1.3699e-02	5.8966e-04	5.8211e-03	2.1526e-04	1.2347

Table 9
Second-order in space and first-order IMEX in time. Refined mesh. The last cell of size $\Delta x = 0.1$ was now divided in three cells of sizes respectively $\Delta x_1 = 0.01, \Delta x_2 = 0.01,$ and $\Delta x_3 = 0.08$.

α	E_1	Δt	E_2	Δt	Rate
0.9	9.5457e-03	3.7577e-04	2.2271e-03	1.7234e-04	2.0997
0.7	9.7531e-03	3.2782e-05	2.2869e-03	1.2032e-05	2.0924

Table 10
Rate of convergence, when $T = 1$, for a smooth solution, with $\Delta x = \Delta v = 1/800$ and $M = 5$ and $M = 10$. The convergence rate in time is $2 - \alpha$ as expected.

α	E_1	E_2	Rate
0.7	1.3214e-02	5.2850e-03	1.3221
0.5	5.9018e-03	2.0013e-03	1.5602
0.3	2.1402e-03	6.3645e-04	1.7496

The last test, displayed in Table 9, illustrates how the second-order accuracy can be recovered by refining the mesh near the boundary. Now, for the second-order IMEX method with the fictitious cells we consider a non-uniform mesh. In particular we consider for the cells near the left boundary $\Delta x_1 = 0.01,\ \Delta x_2 = 0.01$ and $\Delta x_3 = 0.08$ to replace the cell of size $\Delta x = 0.1$. In the right part of the domain we have proceeded similarly by choosing $\Delta x_{N_x-2} = 0.01,\ \Delta x_{N_x-1} = 0.01$ and $\Delta x_{N_x} = 0.08$ to refine $\Delta x = 0.1$.

5.4. Order of convergence in time

In this subsection, the test examples show the rates of convergence regarding time. They depend on the regularity of the solution and the time steps of the mesh, in particular, if they are uniform or non-uniform. Only the implicit method is implemented, since the purpose of this section is to show the convergence rate in time.

In the next tables we present the errors between the exact solution and the numerical solution given by (47) and the rates of convergence in time are measured according to

$$\text{Rate} = \frac{\log(E^{M}_{N_x,N_v}) - \log(E^{\tilde{M}}_{N_x,N_v})}{\log(\tilde{M}) - \log(M)}, \tag{48}$$

with $M < \tilde{M}$. The number of grid points in time M and $\tilde{M}$ are associated with two meshes that keep the same number of space and phase discrete points N_x and N_v respectively.

Consider the Klein-Kramers equation with homogeneous boundary conditions. The variables and the source term are the same as in Section 5.1. The space and phase steps are now $\Delta x = \Delta v = 1/800$ and the uniform time steps obtained with $M = 5$ and $M = 10$. For this example the solution in time is $C^2[0, T]$ and therefore a convergence rate of $2 - \alpha$ is expected, as proved in [27]. The rates of convergence are displayed in Table 10 and they are according to this result.

In the next example, the regularity of the solution is decreased. Consider the Klein-Kramers equation defined in $(x, v) \in [0, 2] \times [0, 2]$ and $t \in [0, T]$, with $T = 1$, $D = 1$, $\gamma = 1$ and $F(x, v) = x^2 - v$. A source term is assumed on the right-hand side of the equation, in order to be able to get an exact solution, that is given by $u(x, v, t) = (t^\alpha + t^3)v^4x^4(2 - x)^4(2 - v)^4$.

An uniform mesh in x and v is considered with $\Delta x = 1/800$ and $\Delta v = 1/800$ and uniform time steps with $M = 25$ and $M = 50$. For this case, the expected rate of convergence is α, see [39]. In Table 11 we observe that a slightly lower rate than α is obtained.

In Tables 12 and 13, the results for a non-uniform graded mesh of the form $t_n = T(n/M)^r$ are shown and it illustrates how the convergence rate improves as discussed in [26,39]. We consider $r = 1/\alpha$ in Table 12 and $r = (2 - \alpha)/\alpha$ in Table 13. For the first case the rate of convergence improves to 1 and for the second case it improves to $2 - \alpha$.

Table 11
Rate of convergence, when $T = 1$, for a less smooth solution with $\Delta x = \Delta v = 1/800$ and a uniform time step with $M = 25$ and $M = 50$. The convergence rate in time is nearly α, the expected value.

α	E_1	E_2	Rate
0.7	9.0378e-03	6.0426e-03	5.8080e-01
0.5	1.7038e-02	1.3313e-02	3.5589e-01
0.3	2.1272e-02	1.9039e-02	1.5997e-01

Table 12
Rate of convergence, when $T = 1$, for a less smooth solution with $\Delta x = \Delta v = 1/800$ and a graded mesh $t_n = T(n/M)^{1/\alpha}$ with $M = 25$ and $M = 50$. The convergence rate in time improved to 1 when compared with the rate for a uniform time step shown in the previous table.

α	E_1	E_2	Rate
0.7	4.7996e-03	2.2580e-03	1.0878
0.5	4.5949e-03	2.4136e-03	9.2885e-01
0.3	3.9422e-03	2.0726e-03	9.2756e-01

Table 13
Rate of convergence, when $T = 1$, for a less smooth solution with $\Delta x = \Delta v = 1/800$ and a graded mesh $t_n = T(n/M)^{(2-\alpha)/\alpha}$ with $M = 25$ and $M = 50$. The convergence rate in time improved to $2 - \alpha$.

α	E_1	E_2	Rate
0.7	6.7659e-03	2.4771e-03	1.4496
0.5	4.8932e-03	1.5497e-03	1.6588
0.3	4.3798e-03	1.3123e-03	1.7388

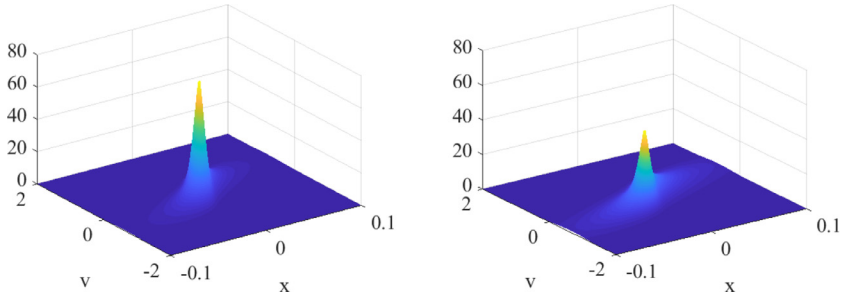

Fig. 7. Initial condition (49) with $\epsilon = 0.005$. The force field is $F_{\text{ext}}(x) = 0$. The parameters are $D = 1$, $\gamma = 1$ and $\alpha = 0.8$. From left to right the time increases: Left: $T = 0.06$. Right: $T = 0.1$.

5.5. Numerical solutions for different force fields

Numerical solutions for the Klein-Kramers equation are presented for different force fields. The initial condition is specified by a Gaussian function, located in the middle of the domain

$$u_0(x, v) = \frac{1}{\epsilon\sqrt{\pi}} \mathrm{e}^{-(x-c)^2/\epsilon^2} \frac{1}{\epsilon\sqrt{\pi}} \mathrm{e}^{-v^2/\epsilon^2}, \quad c = \frac{x_L + x_R}{2}, \tag{49}$$

for a small value of ϵ. When ϵ goes to zero the initial condition approaches the Dirac delta function and the solutions of the fractional Klein-Kramers equation represent probability distribution functions.

To exemplify that we can use this methodology to obtain numerical approximations for probability distribution functions of physical interest we start to display numerical solutions for two cases presented in [29], where two types of potentials have been studied, namely, a constant potential and a double-well potential, that is, the force fields are

$$F_{\text{ext}}(x) = 0 \quad \text{and} \quad F_{\text{ext}}(x) = -\frac{d}{dx}\left(\frac{x^4}{4} - 2x^2\right)$$

respectively. In these cases we consider an open domain. In Fig. 7 we display the solutions for $F_{\text{ext}}(x) = 0$ and in Fig. 8 for $F_{\text{ext}}(x) = -x^3 + 4x$. In Fig. 8, the stationary solution at $T = 30$ can be seen as well as the two stable states at $x = \pm 2$. This stationary solution is according to the discussion in [29].

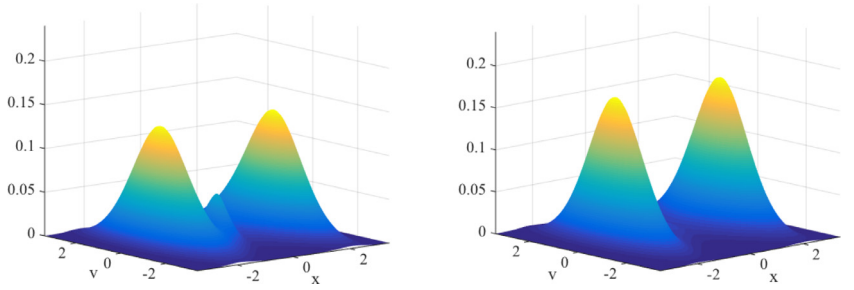

Fig. 8. Initial condition (49) with $\epsilon = 0.2$. The force field is $F_{\text{ext}}(x) = -x^3 + 4x$, $D = 1$, $\gamma = 1$, $\alpha = 0.9$. Left: $T = 5$. Right: $T = 30$. The stationary solution is visible for $T = 30$ where we observe the two stable states at $x = \pm 2$.

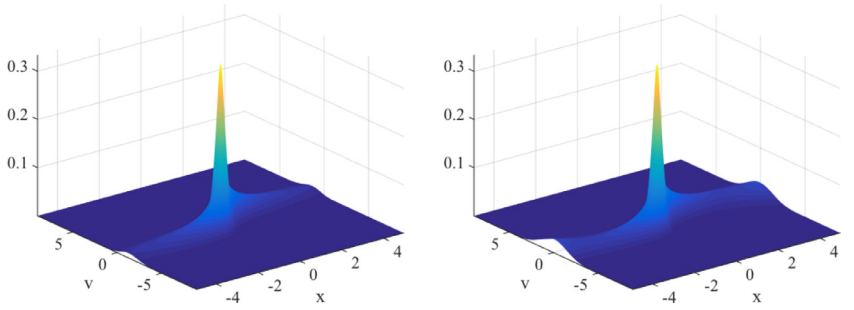

Fig. 9. Initial condition (49) with $\epsilon = 0.2$. The force field is the derivative of the minus modulus. Spatial domain $-5 < x < 5$, $D = 1$, $\gamma = 1$, $\alpha = 0.3$, $T = 20$. Left: Absorbing boundary conditions. Right: Reflecting boundary conditions.

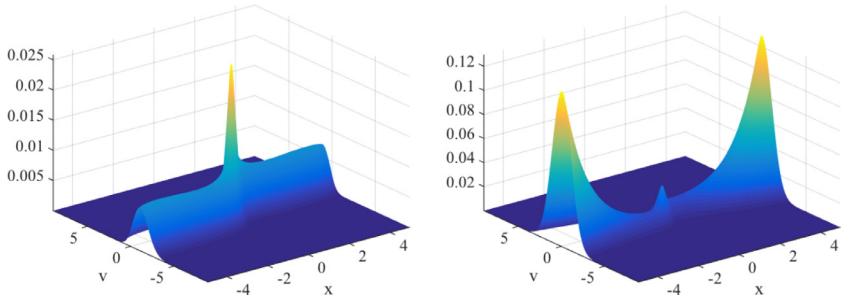

Fig. 10. Initial condition (49) with $\epsilon = 0.2$. The force field is the derivative of the minus modulus. Spatial domain $-5 < x < 5$, $D = 1$, $\gamma = 1$, $\alpha = 0.8$, $T = 20$. Left: Absorbing boundary conditions. Right: Reflecting boundary conditions.

Other force fields also of physical interest are

$$F_{\text{ext}}(x) = -\frac{d}{dx}(-|x|) \quad \text{and} \quad F_{\text{ext}}(x) = -\frac{d}{dx}(\cos(8\pi x/10)).$$

Numerical solutions are displayed in Figs. 9–12 and for these cases absorbing and reflecting boundaries have been included. The initial condition considered is (49) with $\epsilon = 0.2$ and the parameters are $\gamma = 1$, $D = 1$. The solutions are shown for two different values of α, that is, $\alpha = 0.3$ and $\alpha = 0.8$. The solutions are strongly influenced by the force fields and the boundary conditions. In Figs. 9–10, the numerical solutions for the minus modulus potential field are plotted when $T = 20$ and $\alpha = 0.3$ and $\alpha = 0.8$. In Figs. 11–12, the numerical solutions for the periodic potential field are plotted when $T = 50$, and for the same values of α as the previous example.

We proceed to compare the performance of the implicit finite volume method discussed in this work with the finite difference method presented in [6] for the open domain. The non-oscillatory behaviour of the computed solution is demonstrated in Fig. 13, that is, it can be observed that no spurious oscillations are formed when the positivity preserving finite volume method is used in opposition to what happens with the finite difference method. The numerical solutions are computed for the periodic potential defined above, $T = 30$ and different values of the parameter D. The oscillatory behaviour can be seen when the solution is computed with the finite difference method, for small values of D.

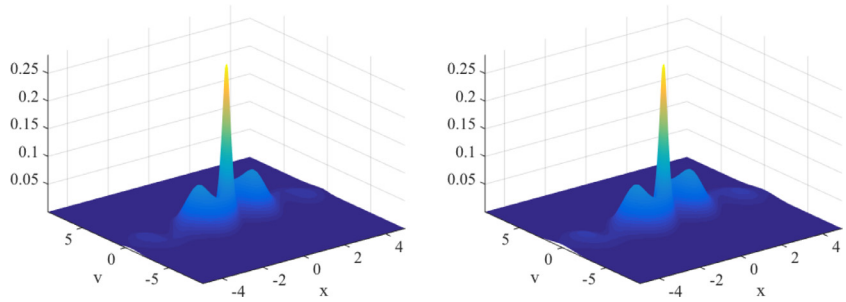

Fig. 11. Initial condition (49) with $\epsilon = 0.2$. The force field is the derivative of a periodic potential. Spatial domain $-5 < x < 5$, $D = 1$, $\gamma = 1$, $\alpha = 0.3$, $T = 50$. Left: Absorbing boundary conditions. Right: Reflecting boundary conditions.

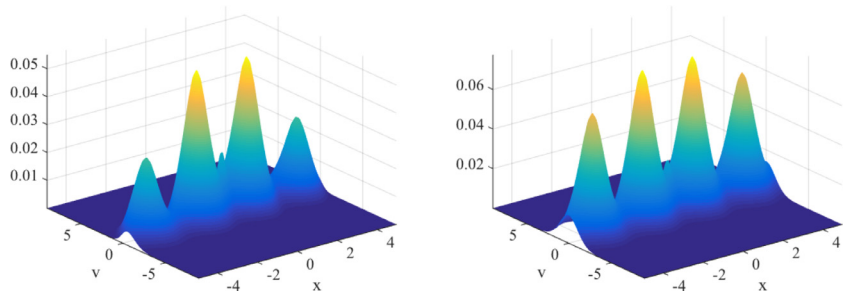

Fig. 12. Initial condition (49) with $\epsilon = 0.2$. The force field is the derivative of a periodic potential. Spatial domain $-5 < x < 5$, $D = 1$, $\gamma = 1$, $\alpha = 0.8$, $T = 50$. Left: Absorbing boundary conditions. Right: Reflecting boundary conditions.

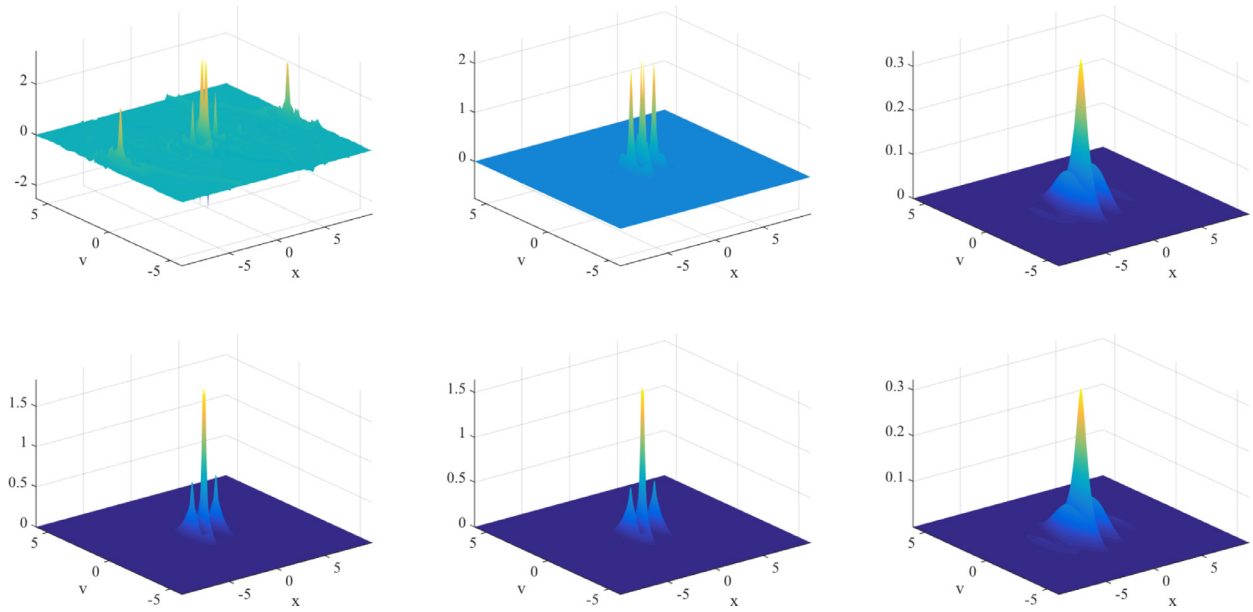

Fig. 13. Top: Numerical solution computed with the finite difference method [6]. Bottom: Numerical solution computed with the finite volume method. Initial condition (49) with $\epsilon = 0.2$. The force field is the derivative of a periodic potential. Open domain with $\gamma = 1$, $\alpha = 0.3$, $T = 30$, $\Delta x = \Delta v = 0.1$, $\Delta t = 0.05$. From left to right the diffusion increases: $D = 0.001$, $D = 0.01$, $D = 1$.

6. Conclusions

A family of finite volume schemes have been implemented that includes first and second-order methods in phase space and are explicit or implicit in time. We have seen that explicit methods impose restrictive conditions for the cases when α is less than 0.5 and therefore the development of implicit methods in this context is of importance. Explicit methods, presented in the literature, for differential equations that involve a fractional derivative in time, show this limitation. We

have also considered absorbing and reflecting boundaries that lead us to a different formulation of the numerical approach near the boundaries. This formulation had an influence on the lost of accuracy of the overall numerical method. However, it was shown that the lost of accuracy can be recovered with the use of non-uniform meshes.

Declaration of Competing Interest

The authors declare that they have no known competing financial interests or personal relationships that could have appeared to influence the work reported in this paper.

CRediT authorship contribution statement

Luís Pinto: Methodology, Software, Formal analysis, Validation, Visualization, Writing - original draft. **Ercília Sousa:** Conceptualization, Methodology, Formal analysis, Validation, Visualization, Writing - original draft.

Acknowledgments

The authors would like to thank the reviewers and the editor for their comments that allowed us to improve the quality of the manuscript.

References

[1] Araújo A, Das AK, Sousa E. A numerical approach to study the kramers equation for finite geometries: boundary conditions and potential fields. J Phys A 2015;48:045202.
[2] Barkai E, Silbey J. Fractional kramers equation. Phys Chem B 2000;104:3866–74.
[3] Berman A, Plemmons RJ. Nonnegative matrices in mathematical sciences. SIAM 1994.
[4] Bodrova AS, Chechkin AV, Cherstvy AG, Safdari H, Sokolov IM, Metzler R. Underdamped scaled brownian motion: (non-)existence of the overdamped limit in anomalous diffusion. Sci Rep 2016;6:30520.
[5] Chertock A, Kurganov A. A second-order positivity preserving central-upwind scheme for chemotaxis and haptotaxis models. Numer Math 2008;111:169–205.
[6] Deng W, Li C. Finite difference methods and their physical constraints for the fractional Klein-Kramers equation. Numer Methods Partial DifferEqs 2011;27:1561–83.
[7] Diethelm K, Ford NJ, Freed AD, Luchko Y. Algorithms for the fractional calculus: a selection of numerical methods. Comput Methods Appl Mech Eng 2005;194:743–73.
[8] Duan B, Zheng Z. An exponentially convergent scheme in time for time-fractional diffusion equations with non-smooth initial data. J Sci Comput 2019;80:717–42.
[9] El-Sayed AA, Agarwal P. Numerical solution of multiterm variable-order fractional differential equations via shifted Legendre polynomials. Math Method Appl Sci 2019;42:3978–91.
[10] Fok JCM, Guo B, Tang T. Combined hermite spectral-finite difference method for the Fokker-Planck equation. Math Comput 2002;71:1497–528.
[11] Guo YB, Wang TJ. Composite generalized Laguerre-Legendre spectral method with domain decomposition and its application to Fokker-Planck equation in an infinite channel. Math Comput 2009;78:129–51.
[12] Gadja J, Magdziarz M. Kramers escape problem for fractional Klein-Kramers equation with tempered α-stable waiting times. Phys Rev E 2011;84:021137.
[13] Hendy AS, Macías-Díaz JE. A novel discrete Gronwall inequality in the analysis of difference schemes for time-fractional multi-delayed diffusion equation. Commun Nonlinear Sci Numer Simul 2019;73:110–19.
[14] Hunsdorfer W, Ruuth SJ, Spiteri RJ. Monotonocity-preserving linear multistep methods. SIAM J Numer Analys 2003;41:605–23.
[15] Hunsdorfer W, Verwer JG. Numerical solution of time-dependent advection-diffusion-reaction equations. Springer; 2003.
[16] Jiang GS, Tadmor E. Non-oscillatory central schemes for multidimensional hyperbolic conservation laws. SIAM J Sci Comput 1998;19:1892–917.
[17] Jiang Y, Xu X. A monotone finite volume method for time fractional Fokker-Planck equations. Sci China Math 2019;62:783–94.
[18] Jin B, Lazarov R, Zhou Z. An analysis of the l1 scheme for the subdiffusion equation with nonsmooth data. IMA J Numer Anal 2016;36:197–221.
[19] Kilbas AA, Srivastava HM, Trujillo JJ. Theory and applications of fractional differential equations. Elsevier; 2006.
[20] Klein O. Zur statistischen theorie der suspensionen und lsungen. Arkiv för Matematik Astronomi och Fysik 1921;16:1–51.
[21] Kopteva N. Error analysis of the $l1$ method on graded and uniform meshes for a fractional derivative problem in two and three dimensions. Math Comput 2019;88:2135–55.
[22] Kramers AH. Brownian motion in a field of force and the diffusion model of chemical reactions. Physica 1940;7:284–304.
[23] Kurganov A, Tadmor E. New high-resolution central schemes for nonlinear conservation laws and convection-diffusion equations. J Comput Phys 2000;160:241–82.
[24] Kurganov A, Noelle S, Petrova G. Semidiscrete central-upwind schemes for hyperbolic conservation laws and Hamilton-Jacobi equations. SIAM J Sci Comput 2001;23:707–40.
[25] Li C, Zhang F. Numerical methods for fractional calculus. Chapman & Hall/CRC Press; 2015.
[26] Liao HL, Li D, Zhang J. Sharp error estimate of the nonuniform $l1$ formula for linear reaction-subdiffusion equations. SIAM J Numer Anal 2018;56:1112–33.
[27] Lin X, Xu C. Finite difference/spectral approximations for the time-fractional diffusion equation. J Comput Phys 2007;225:1533–52.
[28] Liu JG, Ma Z, Zhou Z. Explicit and implicit TVD schemes for conservation laws with Caputo derivatives. J Sci Comput 2017;72:291–313.
[29] Magdziarz M, Weron A. Numerical approach to the fractional Klein-Kramers equation. Phys Rev E 2007;76:066708.
[30] Mendes EMAM, Salgado GHO, Aguirre LA. Numerical solution of Caputo fractional differential equations with infinity memory effect at initial condition. Commun Nonlinear Sci Numer Simul 2019;69:237–47.
[31] Metzler R, Klafter J. The random walk's guide to anomalous diffusion: a fractional dynamics approach. Phys Rep 2000;339:1–77.
[32] Metzler R, Klafter J. From a generalised Chapman-Kolmogorov equation to the fractional Klein-Kramers equation. J Phys Chem B 2000;104:3851.
[33] Metzler R, Klafter J. Subdiffusive transport close to thermal equilibrium: from the Langevin equation to fractional diffusion. Phys Rev E 2000;61:6308.
[34] Oldham KB, Spanier J. The fractional calculus. Dover; 1974.
[35] Orze S, Weron A. Fractional Klein-Kramers dynamics for subdiffusion and Itô formula. J Stat Mech Theory E 2011;2011:P01006.
[36] Pinto L, Sousa E. Numerical solution of a time-space fractional Fokker planck equation with variable force field and diffusion. Commun Nonlinear Sci Numer Simul 2017;50:211–28.
[37] Risken H. The Fokker-Planck equation. Springer; 1989.

[38] Samko SG, Kilbas AA, Marichev OI. Fractional integrals and derivatives: theory and applications. Gordon and Breach Science Publishers; 1993.
[39] Stynes M, O'Riordan E, Gracia JL. Error analysis of a finite difference method on graded meshes for a time-fractional diffusion equation. SIAM J Numer Anal 2017;55:1057–79.
[40] Tawfik AM, Fichtner H, Elhanbaly A, Schlickeiser R. An analytical study of fractional Klein-Kramers approximations for describing anomalous diffusion of energetic particles. J Stat Phys 2019;174:830–45.